NIPER-235
(DE88001237)

EFFECT OF RESERVOIR HETEROGENEITIES ON WATERFLOOD AND EOR CHEMICAL FLOOD PERFORMANCE

Topical Report

By
Liviu Tomutsa
Jeff Knight

October 1988

Performed Under Cooperative Agreement No. FC22-83FE60149

IIT Research Institute
National Institute for Petroleum and Energy Research
Bartlesville, Oklahoma

Bartlesville Project Office
U. S. DEPARTMENT OF ENERGY
Bartlesville, Oklahoma

DISCLAIMER

This report was prepared as an account of work sponsored by an agency of the United States Government. Neither the United States Government nor any agency thereof, nor any of their employees, makes any warranty, express or implied, or assumes any legal liability or responsibility for the accuracy, completeness, or usefulness of any information, apparatus, product, or process disclosed, or represents that its use would not infringe privately owned rights. Reference herein to any specific commercial product, process, or service by trade name, trademark, manufacturer, or otherwise, does not necessarily constitute or imply its endorsement, recommendation, or favoring by the United States Government or any agency thereof. The views and opinions of authors expressed herein do not necessarily state or reflect those of the United States Government or any agency thereof.

Printed in the United States of America. Available from:
National Technical Information Service
U.S. Department of Commerce
5285 Port Royal Road
Springfield, VA 22161

NTIS price codes
Paper copy: **A05**
Microfiche copy: **A01**

NIPER-235
Distribution Category UC-122

EFFECT OF RESERVOIR HETEROGENEITIES ON WATERFLOOD AND EOR CHEMICAL FLOOD PERFORMANCE

Topical Report

By
Liviu Tomutsa
Jeff Knight

October 1988

Work Performed Under Cooperative Agreement No. FC22-83FE60149

Prepared for
U.S. Department of Energy
Assistant Secretary for Fossil Energy

E.B. Nuckols, Project Manager
Bartlesville Project Office
P.O. Box 1398
Bartlesville, OK 74005

Prepared by
IIT Research Institute
NATIONAL INSTITUTE FOR PETROLEUM AND ENERGY RESEARCH
P.O. Box 2128
Bartlesville, OK 74005

TABLE OF CONTENTS

Page

Abstract....1
Introduction....2
Literature Review....4
Acknowledgments....9
Two Dimensional (2D) Waterflood Simulation Sensitivity Studies....10
Discussion of 2D Simulator Results....11
Three Dimensional Waterflood Simulations....15
Description of Chemical Flood Simulator....16
Model Formulation and Solution Procedure....16
Limitations of Available Version of Micellar-Polymer Simulator....17
Summary and Conclusions....18
References....20
Appendix A - Boast Code Modifications....70
Appendix B - Residual Oil Saturation Graphics Program....76

TABLES

1. Empirical Data....25
2. Slopes for Compressibility Calculations....26
3. Run Control Parameters....27
4. Code for ROS Distribution Displays (Figs. 1-22)....28
5. Code for ROS Differences....29
6. High Permeability Center Layers Cases....30
7. Low Permeability Center Layers Cases....31
8. Regressive and Progressive Sequences Simulations....32
9. Run Time Studies....33

ILLUSTRATIONS

1. ROS Distribution 2D (k_h = 346.5 md)....34

2. ROS Distribution 2D (k_h = 265 md layer 1,2,3,7,8,9,10) (k_h = 533 md layer 4,5,6)....35

3. ROS Distribution 2D (k_h = 93.6 md layer 1,2,3,7,8,9,10) (k_h = 939 md layer 4,5,6)....36

4. ROS Distribution 2D (k_h = 11.3 md layer 1,2,3,7,8,9,10, k_h = 1129 md layer 4,5,6)....37

5. ROS Distribution 2D (k_h = 407 md layer 1,2,3,7,8,9,10, k_h = 203 md layer 4,5,6)....38

6. ROS Distribution 2D (k_h = 474 md layer 1,2,3,7,8,9,10, k_h = 47.5 md layer 4,5,6)....39

7. ROS Distribution 2D (k_h = 492 md layer 1,2,3,7,8,9,10, k_h = 4.92 md layer 4,5,6)....40

8. ROS Distribution 2D (k_h/k_z = 1, k_h = 346.5 md)....41

TABLE OF CONTENTS (Continued)

9. ROS Distribution 2D (k_h/k_z = 5, k_h = 346.5 md).....42

10. ROS Distribution 2D (k_h/k_z = 40, k_h = 346.5 md).....43

11. ROS Distribution 2D (k_h = 462 md layer 1 - 5, k_h = 231 md layer 6-10, 10% shale between layer 5 and 6).....44

12. ROS Distribution 2D (k_h = 462 md layer 1-5, k_h = 231 md layer 6-10, 40% shale between layer 5 and 6).....45

13. ROS Distribution 2D (k_h = 462 md layer 1-5, k_h = 231 md layer 6-10, 100% shale between layers 5 and 6).....46

14. ROS Distribution 2D (k_h = 630 md layer 1-5, k_h - 63 md layer 5-10 10% shale between layers 5 and 6).....47

15. ROS Distribution 2D (k_h = 630 md layer 1-5, k_h = 63 md layer 6-10 40% shale between layers 5 and 6).....48

16. ROS Distribution 2D, Case A (k_h = 346.5 md).....49

17. ROS Distribution 2D, Case B ($k_{htop}/k_{hbottom}$ = 5, k_{htop} = 662.5 md).....50

18. ROS Distribution 2D, Case C ($k_{htop}/k_{hbottom}$ = 1/5, k_{htop} = 132.5 md)....51

19. ROS Distribution 2D, Case D ($k_{htop}/k_{hbottom}$ = 25, k_{htop} = 975.1 md).....52

20. ROS Distribution 2D, Case E ($k_{htop}/k_{hbottom}$ = 1/25, k_{htop} = 39 md).....53

21. ROS Distribution 2D, Case F ($k_{htop}/k_{hbottom}$ = 100, k_{htop} = 1189 md).....54

22. ROS Distribution 2D, Case G ($k_{htop}/k_{hbottom}$ = 1/100, k_{htop} = 11.9 md)...55

23. Cumulative oil production (layers 5,6 of variable permeability: A) 300 md, B) 450 md, C) 600 md, D) 1500 md, E) 3000 md, F) 6000 md.....56

24. Cumulative oil production, (layers 4,5,6 of variable permeability. Letter codes same as FIG. 23.).....57

25. ROS differences between homogeneous case and layer 5 of varied permeabilities after 2 yrs of waterflood (A) 450 md, B) 600 md, C) 1500 md, C) 3000 md, D) 6000 md.....58

26. Number of time steps vs waterflood time (layers 4,5,6 of variable permeability: a) 300 md, B) 600 md, C) 6000 md.).....59

27. Cumulative oil production (k_h/k_z = 1(A), 2(B), 4(C), 10(D), 20(E), 40(F).....60

28. Effect of vertical permeability on number of simulation time steps.....61

TABLE OF CONTENTS (Continued)

Page

29. Cumulative oil production. Effect of vertical variation in layer permeability (k_{top}/k_{bottom} = 1(A), 5(B), 1/5(C), 25(D), 1/25(E), 100(F), 1/100(G)).....62

30. Two inverted five spot configurations.....63

31. ROS Distributions 3D case waterflood, year 4 (A-E: horizontal layers 1-5 (top to bottom) F-H: vertical yz cross sections from most outward cross section (F) toward cross section through injector wells (H).....64

32. ROS Distributions 3D case; waterflood year 10 (same cross sections as in FIG. 31.).....67

TOPICAL REPORT

EFFECT OF RESERVOIR HETEROGENEITIES ON WATERFLOOD AND EOR CHEMICAL FLOOD PERFORMANCE

By Liviu Tomutsa* and Jeff Knight+

ABSTRACT

Simulations were performed to study the capability of a modified version of the black oil simulator BOAST to handle reservoir heterogeneities of the type encountered in the barrier bar depositional system studied in the geoscience research program being performed for the Department of Energy as project BE1. The cases studied consisted of two-dimensional and three-dimensional simulations of layered reservoirs with different permeability contrasts between the layers, different vertical permeability /horizontal permeability ratios and continuous and discontinuous shale layers.

To understand the effect of heterogeneities on residual oil location, software was developed to show graphically the residual oil saturation in the reservoir grid blocks at selected time intervals during the simulation. BOAST was modified for the residual oil saturation displays as well as for graphical displays of production rates and cumulative production versus time of oil, water and gas.

We found that BOAST can adequately handle the type and range of permeability variations and contrasts studied; however, the increase in run time/simulation limits the number of grid blocks that can be processed to less than 2,000 when the Microvax II computer is used. To reduce the computation time, thin layers with permeability ratios of 2 or less or with vertical permeability to horizontal permeability ratios larger than 4 could be combined into single layers with only a small effect on the residual oil distribution and the oil production rates. High permeability contrasts in transgressive or

*Research physicist.
+Consultant.

regressive sequences cause early water breakthrough and low cumulative oil production, with the transgressive permeability cases being worse. A single, discontinuous layer of shale does not significantly effect the simulation results.

Additional simulations will be conducted to include the effect of relative permeabilities and capillary pressures of each layer.

Applicability and limitations of the micellar-polymer simulator for investigation of the effect of reservoir heterogeneities on chemical floods are outlined.

INTRODUCTION

One of the major goals of the geoscience research at NIPER is to improve the understanding of the magnitude and location of the residual oil in reservoirs belonging to the barrier bar deposystems. The research program makes use of reservoir data, outcrop data and simulation results to identify the effect of various heterogeneities on oil flow and oil trapping in barrier bar reservoirs. After heterogeneities were identified from preliminary geological and production investigations, computer simulations, using a black oil simulator, were conducted (a) to evaluate our capabilities to handle these heterogeneities and (b) to acquire a more quantitative understanding of the effect of various heterogeneities on the reservoir fluid movement.

The purpose of the present work is to

1. review the previous work concerning reservoir heterogeneity effects on waterflood and chemical flood simulations;
2. conduct sensitivity studies with emphasis on residual oil saturation (using a simulator readily available to NIPER) for heterogeneities of the type present in the barrier island deposystem selected for study in project BE1; and
3. make recommendations concerning the degree of detail necessary to adequately describe reservoirs for waterflooding or chemical flooding.

To simulate accurately on a large scale the movement and retention of fluids in a petroleum reservoir, accurate descriptions of the properties of the reservoir rocks, the reservoir fluids, and their microscopic interactions are required.

For black oil waterflood simulation, the following rock parameters are needed: rock depth; thickness; permeability vector (or tensor); porosity; transmissibility vector (or tensor) between grid blocks; rock compressibility; oil, water, and gas relative permeabilities; and capillary pressures.

The following fluid PVT properties should be specified:

1. Oil PVT properties -- initial bubblepoint pressure; the tables of variation with pressure of oil viscosity, oil formation volume factor, and solution gas-oil ratio for undersaturated oil; and the tables of variation with pressure of viscosity, formation volume factor, and solution gas-oil ratio for the saturated oil.
2. Water PVT properties -- tables of variation with pressure of viscosity, formation volume factor, and solution gas-water ratio.
3. Gas PVT properties -- tables of variation with pressure of viscosity and formation volume factor.
4. Stock tank fluid densities for oil and water; initial pressure; oil, water, and gas saturation distributions; and well information data (location of injectors and producers, flow rates or bottomhole flowing pressures, completion depth and interval and the productivity index).

The simulation output consists of: fluid flow rates, cumulative fluid production, water-oil and gas-oil ratios for each layer and totals for each well. The output also contains the spatial distribution in the reservoir of the pressure, water saturation, residual oil saturation and gas saturation.

For chemical flood simulation, other data should be added to the above, for example:

1. salinity of the reservoir brine, preflush and chemical (and/or polymer) slug;
2. injection rates and duration of the preflush, chemical and/or polymer slug;
3. phase behavior of the chemical slug with oil versus the salinity and chemical concentration;
4. viscosity of the chemical slug and the polymer slug;
5. adsorption coefficient of the surfactant and polymer;
6. cation exchange capacity;

7. interfacial tension data as a function of salinity.

The reservoir heterogeneities are described by variations in the rock-related parameters throughout the reservoir: permeability, porosity, relative permeability, capillary pressure, and rock compressibility.

Rock parameters are often measured on much smaller volumes than the simulator grid blocks. Furthermore, the measurements are obtained only at well locations throughout the reservoir. Therefore, mathematical methods which consider the type of flow process and the spatial distribution of different rock types in the reservoir must be used to predict the values of these parameters for the simulator grid block volumes (scaleup process) and at locations where no samples are taken (interpolation process). Depending upon the rock distribution, either deterministic or statistical methods are used in the scaleup and interpolation processes.

Literature Review

As early as the 1940s, Suder[1] and Stiles[2] presented analytical methods which incorporate the effect of permeability variations on oil recovery, by rearranging the permeabilities in decreasing order and using the new permeability distribution for calculating the average waterflood recovery for a given field. Muskat[3] showed analytically that the performance of an idealized (neglecting crossflow) stratified reservoir under waterflood depends upon water-oil mobility ratios and stratification ratios. Schmaltz and Rahme[4] extended the findings of Suder and Stiles to different permeability distribution arrays and described the relationship between the amount of recoverable oil and the Lorentz coefficient of heterogeneity for permeabilities. This relationship provides a preliminary estimation of expected performance of a waterflood.

Dykstra and Parsons[5] have defined a heterogeneity coefficient which has also been used frequently to estimate oil recovery from waterfloods. The use of the Lorentz coefficients, Dykstra-Parsons coefficient, and other graphical methods in estimating waterflood performance is summarized by Neil, et al.[6] Koval[7] has used the Dykstra-Parsons coefficient to predict the performance of miscible displacement in hetergeneous media. More recent work by Jensen and Lake[8] shows the relationship between the error observed when using these methods and the number of core samples used in the calculations.

Warren and Price[9] have used Monte Carlo numerical simulations to study the effect of 3-dimensional (3D), spatially random permeability distributions. They have found that "the most probable behavior of a heterogeneous system with single-phase flow approaches that of a homogeneous system having a permeability equal to the geometric mean of the individual permeabilities" of the heterogeneous system. They also found that "the permeability determined from a pressure buildup test of a hetergeneous reservoir gives a reasonable value for the effective permeability within the drainage area."

Warren and Skiba[10] have extended the Monte Carlo study of effect of spatially random permeability distributions to three dimensional miscible flooding. They have found that the effect of porosity variations on macroscopic dispersion is second order compared to the effect of permeability variations, and that a unique characterization of the reservoir cannot be obtained from field performance data and core analysis data alone unless the displacement mechanism is known unequivocally. They postulated a minimum-data method based on core analysis and pressure buildup tests for estimating the spatial distribution of permeabilities.

The waterflood behavior in a stratified system was studied by Warren and Cosgrove[11] using analytical formulations for a discrete, uniform layered reservoir with negligible capillary and gravitational forces compared to viscous forces and for a piston-like displacement. Their method predicts a lower vertical sweep efficiency with an unfavorable mobility ratio and a higher vertical sweep efficiency with a favorable mobility ratio compared to vertical sweep efficiencies predicted using the Dykstra-Parsons method. They show that the effect of crossflow in a stratified reservoir can be appreciable, especially when either extremely favorable or unfavorable mobility ratios exist. On a small scale, Huppler[12] studied the effect of core heterogeneities on waterflood relative permeabilities. Heterogeneities studied were horizontal and vertical layers and spatially distributed high- and low-permeability lenses and vugs. He found that while evenly distributed heterogeneities or minor permeability contrasts (smaller than 2:1) show large-scale homogeneous behavior, the effect of channel-like heterogeneities results in significant effects. Such heterogeneities cause waterflood results to be sensitive to flooding rates, core lengths, and wetting characteristics. Measuring permeability in cores by direct and reverse flow and averaging the results was recommended.

For simulations of stratified reservoirs, Hearn[13] calculated pseudo relative permeabilities. He assumed that incompressible flow and piston-like displacement occurred independently in each layer and that these were a negligible vertical pressure gradient compared to the horizontal gradient. Hawthorne[14] modified Hearn's model to include capillary pressure effects. Jacks, et al.[15] and Kyte and Bery[16] calculated dynamic pseudo functions (time-dependent) which allowed simulation of three dimensional (3D) models using two dimensional (2D) simulators in nonequilibrium cases (poor vertical communication, changes in flowrates, etc.) including pseudo capillary pressures. Kortekaas[17] calculated the relative permeability and capillary pressure of repetitive zones of alternating permeabilities representing crossbedded sandstone. The pseudofunctions generated were used in waterflood simulations. He found that neglecting the crossbedding produces optimistic simulation results, and that much oil is left behind in the higher permeability foreset laminae when the fluid flow occurs perpendicularly to them.

Lake and Hirasaki[18] have found that the transverse dispersion of a two-layer medium is bound by that of a two-layer medium with dispersion occurring only longitudially within each layer and that of a single-layer medium having an augmented longitudial dispersion coefficient. The transverse dispersion number indicates where between the two extremes the displacement lies. For a multilayer system, a grouping procedure for the layers is described.

The effect of random shales on reservoir simulation was studied by Haldorsen and Lake.[19] They described a new statistical procedure to generate random shales in a reservoir based on cumulative distribution functions for shale length and shale frequency obtained from outcrop and subsurface data for a given depositional environment described by Zeito.[20] Also, they described approximate methods for adjusting the permeability and porosity of large simulator grid blocks containing shales. Martin and Cooper[21] studied the two-phase flow for stochastically generated sand shale sequences and found that the harmonic mean is a poor predictor of effective vertical permeability.

Begg, and King[22] described four methods for establishing the effective vertical permeability (k_{ve}) for single-phase flow in a reservoir containing stochastic shales. They found that k_{ve} is strongly dependent on shale dimensions, shale fractions, and layer thickness and that the results of two-

dimensional models are inappropriate when the major flows are undirectional and normal to the alignment of shales. A review of the engineering problems associated with continuous and stochastic shales, geostatistical techniques to describe and generate shale distributions from outcrops, and the methods to calculate the shale distribution effect on vertical permeability was given by Haldorsen and Chang.[23]

Begg, et al.[24] have generalized the statistical streamline method of Begg and King[22] to a layered medium with different shale statistics and sand permeabilities in each layer. The method was validated in two dimensions (2D) with numerical simulations and measurements on an analog model of an outcrop. Davies and Haldorsen[25] have used pseudofunctions for calculating the relative permeability for waterflood simulator grid blocks containing stochastic shales, with special attention given to the range of volumes over which a pseudofunction can be meaningfully assigned.

White and Horne[26] showed that small simulator grid blocks of different permeability can be replaced by a larger homogeneous grid block for which the transmissibility is a tensor. A tensor-solving algorithm was given and tested for single- and dual-phase flow for shale permeability distribution (vertical cross-section, 2D) and for channel-like permeability distributions (areal, 2D).

The use of permeability tensors for heterogeneous reservoirs with variable directional permeabilities was shown by Shaw and Dawe[27] and Leung.[28] The tensor models for permeability for grid blocks were given. In the first paper, the grid blocks contained heterogeneous patches which were modeled using electrostatic analogues and under certain conditions behaved at large distances like dipoles. This behavior describes the far-field effect of such heterogeneities. Leung's second paper studies the fluid flow in complex reservoirs with multiple zones of various directional permeabilities. The expression for the permeability tensor was validated by simulations for 1D and 2D cases of single-phase flow, and the results are compared to analytical solutions. The tensor method also has the advantage of reducing the effect of grid block orientation on the simulation results.

A systematic approach for handling heterogeneities from small to medium to large scales in two-phase flow was given by Lasseter, et al.[29] They used fractals to describe the small-scale heterogeneities and to generate

pseudofunctions at medium scale. They found that the small-scale heterogeneities have as a main effect, oil trapping, whereas the large-scale heterogeneities control the lateral and vertical communication and that the proper scaleup procedure can affect predicted cumulative oil production by up to 10 percent and can predict earlier water breakthrough.

The effects of permeability stratifications typical for deltaic, channel fill, and beach sand deposits on solution-gas drive and waterflood performance were simulated for a 2D case by Poston and Gross.[30] They found that the transgressive sequence produces the highest recovery in solution-gas drive reservoirs and the serrated and homogeneous sequences produce the highest recovery in waterfloods where high viscosity oil is present. The average residual oil saturation in each layer and producing rate versus recovery relationships for gas drive and waterflood were also calculated.

To determine the effect of heterogeneities on chemical flooding, Arya, et al.[31] have studied by numerical simulation the effect on macroscopic (core size) and megascopic (simulator grid block size) dispersivity by random hetergeneities, aspect ratios, diffusion coefficients, and autocorrelations. The most important factors affecting megascopic dispersion are the heterogeneity (as expressed by the Dykstra-Parsons coefficient), the auto correlation, and the aspect ratio. A classification of heterogeneous media based on length and correlation length into diffusive medium, effectively layered medium, and strictly layered medium was given. Dawe, et al.[32] have studied three-layer cases and rectangular lens cases, both analytically and experimentally (2D glass bead models) of the slug stability in miscible flow. They studied various conductance (permeability/porosity) contrasts between the center layer (or lens) and the rest of the medium and various mobility ratios (M). The experiments and equations developed are applicable to systems where the viscous forces are the dominant factor. They found that a high-permeability layer or lens produces a large finger and small cross flow for $M>1$ and a relatively small effect for $M<1$.

Wheat and Dawe[33] have used numerical simulations and a 2D glass bead laboratory model for the study of transverse dispersion of chemicals in multilayered media of permeability contrasts smaller than 20. The behavior of the slug for different dimensionless times and layer widths is given for unit and non-unit mobility ratios. Novosad[35] performed simulations (with a

modified black oil simulator) and experiments on composite cores made of two slabs (of Berea sandstone and silicone carbide) in capillary contact with each other, both for original water-wet rock and modified oil-wet rock. He found a higher polymer oil recovery from the oil-wet rock than from the water-wet rock, and he determined by how much the absolute oil recovery is higher in the polymer flood than the waterflood for both water-wet and oil-wet rock.

King and Scher[35] showed how to use a "random walk" analysis in the study of both miscible and immiscible floods in a macroscopically homogeneous medium and described a probabilistic simulator. The method could be readily adopted to macroscopically heterogeneous media as it is based on the existence of microscopic heterogeneities which trap and release water and oil "walkers." The flood stability is studied for both a linear and a quarter five-spot example on very fine gridding. The "fingering" and "tip-splitting" effect as a function of mobility ratio is clearly illustrated.

Datta Gupta, et al.[36] have studied micellar-polymer flooding under different conditions of reservoir stratification and mobility ratio. They have used a 3D, multiphase, multicomponent, micellar-polymer simulator to simulate a quarter five-spot with an 11x11x2 grid. Their study confirms that the salinity gradient is the most important factor controlling the performance of the micellar-polymer flood. They found that transverse dispersion and viscous crossflow can mitigate the adverse effect of reservoir heterogeneity on micellar-polymer flood performance, that for small amounts of surfactant injected the size of the slug is not important, and that oil recovery is a strong function of the oil bank/polymer drive mobility ratio. Reducing the mobility ratio from 0.91 to 0.49 increased recovery from 52 to 66 percent. The permeability contrast between layers seems to have only a small influence on the chromatographic separation of the surfactant and alcohol, whereas the salinity gradient has the dominant influence.

ACKNOWLEDGMENTS

N. Maerefat's contribution on the chemical flooding process, the valuable input from M. Honarpour and the contributions by S. Conrad in running simulations and obtaining color plots are acknowledged. The cooperation of the NIPER Computer Center staff in using the Microvax is highly appreciated. The review of this report by Jim Chism of the Department of Energy is appreciated.

The authors are grateful to the Department of Energy for supporting this work through Cooperative Agreement DE-FC22-83FE60149.

TWO DIMENSIONAL SIMULATION SENSITIVITY STUDIES

Based on preliminary evaluation of the geology of the Bell Creek reservoir, the vertical variation in permeability appeared to be the major factor controlling the fluid flow. Most of the simulations were performed on a two dimensional (2D) vertical cross-section with an injector well at one end and a producer well at the other end. To study the effect of large-scale heterogeneities on simulator output, the following cases were studied:

1. Homogeneous base case
2. Higher permeability middle layer(s)
3. Lower permeability middle layer(s)
4. Variations of the vertical permeability
5. Variations of the continuity of a centrally located shale layer
6. Gradual lateral permeability increase with depth
7. Gradual lateral permeability decrease with depth

The effect of reservoir heterogeneities (permeability variation) on the following output variables was studied:

1. Residual oil saturation distribution
2. Time required to develop a predetermined water-oil ratio (WOR) (usually until WOR = 20 was reached.)
3. Number of time steps until WOR = 20
4. Fluid (oil, water, gas) production rates
5. Cumulative fluid (oil, water, gas) production

The waterflood simulator BOAST[37] was used. It is a finite difference implicit pressure-explicit saturation numerical black oil simulator. It was modified to output properly formatted files containing the above variables. The changes are shown in appendix A.

The files were downloaded to an IBM AT computer, and the graphics were displayed on a color screen, black and white or color printer, and a color plotter.

The residual oil saturation distributions were displayed using a graphics program developed for this purpose. We are able to display at specified time intervals 2D cross sections parallel to the xy, xz, and yz planes from a three dimensional (3D) reservoir by assigning different colors or black and white patterns to different residual oil saturation ranges (table 4). Thus, the progression of the waterflood and the location of the unswept or poorly swept area are clearly shown. A listing of the program is shown in appendix B.

The ROS distributions (usually every 1 year, until WOR = 20) for some of the runs performed are shown in figures 1 through 22. The cumulative oil production, production rates, and water oil ratios were plotted with a color plotter. Plots of cumulative oil production versus time are shown in figures 23, 24, 27, and 29.

In the sensitivity studies, the following input parameters were used in the simulators: reservoir dimensions: 400 ft x 200 ft x 50 ft with a grid 40 x 1 x 10; rock porosity, 25 percent; average lateral rock permeability, 346.5 md; average vertical rock permeability, 34.6 md; connate water, 20 percent; initial oil saturation, 80 percent; trapped residual oil saturation, 30 percent; no free gas; bubblepoint pressure, 4,014.7 psi; bottomhole flowing pressure, 4,015 psi; initial reservoir pressure, 4,990 psi (top layer) to 5,002 psi (bottom layer); and depth of the reservoir top, 8,325.5 ft.

The oil, water, and gas data are listed in tables 1 (empirical data) and 2 (slopes for compressibility calculations). The run-control parameters are shown in table 3. The water-injection rate is constant at 100 STB/day, and the production flow index (PID) is 1 for a 346.5-md layer. Because the PID is proportional to the layer permeability, other PID values will be used when the permeability of the layer is different from 346.5 md. The runs stop when the WOR exceeds 20.

DISCUSSION OF 2D SIMULATOR RESULTS

Figure 1 shows the position of the waterbank and the residual oil saturation (ROS) distributions for the base case (k_h = 346.5 md, k_z = 34.65 md). The injector well is at left, the producing well is at the right. Both wells are completed in all the reservoir layers. The darker the shade of gray the higher the oil saturation (table 4B). The top part of figure 1 shows ROS after 1 year of waterflood, and the bottom part shows ROS after 2 years. The

gravity effect is clearly visible, the waterflood advancing faster in the lower part of the reservoir. Figures 2 and 3 also show the position of the waterbank and the ROS after the first and second year of waterflood in figure 4, after only ½ year for the cases when the central three layers (layers 4, 5, and 6) have higher permeability than the top (1, 2, and 3) and bottom (7, 8, and 9) layers. The arithmetic average of the permeability for the 10 layers is the same as that of the homogeneous case (346.5 md). Although a 1:2 permeability ratio (Fig. 2) has only a small effect on the waterbank, ratios 1:10 (Fig. 3) and higher, 1:100 (Fig. 4) have a pronounced effect on the fluid flow. A quick breakthrough in the central layer occurs in the higher permeability cases (before 1 yr, in the 1:100 case), which results in increased water production and a lowering of the cumulative oil production by the time the water-oil ratio equals 20 (table 6). By reducing the permeability of the central layers (by selective plugging), the bypassed oil could be recovered. The effect of permeability variation in the central layers on cumulative oil production is shown in figures 23 and 24. These curves are generated by simulations performed on a 20 x 1 x 10 grid on a 400 ft x 50 ft x 50 ft reservoir and an injection rate of 20 STB/day. The permeability of the central two layers (layers 5 and 6) or central three layers (layers 4, 5, and 6) was varied, and the top and bottom layers were kept constant at k_h = 300 md, k_z = 30 md. The vertical permeability k_z in the central layers was also selected to be 1/10 of lateral permeability k_h.

It is clear from the figures that variations of the order of 2 in the permeability layers, for the layer thickness considered, do not significantly affect oil production, whereas variations by a factor of 4 or more significantly affect oil production, and the effect tapers off with further increases in permeabilities of the central layers (from 3,000 to 6,000 md). These results will serve as a guideline in defining permeability classes and the distinct layers needed for actual reservoir simulations using BOAST. Fig. 25 illustrates, for only 1 layer, the difference in ROS at the end of the waterflood (WOR = 20) between the homogeneous case (300 md) and the heterogeneous cases: (A) 600 md; (B) 1,500 md; (C) 3,000 md; and (D) 6,000 md. The color code is shown in table 5. Only the last two cases (C, D) show significant oil bypassed by the waterflood due to the high-permeability layer. The effect of permeability contrast on the number of time steps required by simulation is shown in figure 26 for the three-layer case. The

one- and two-layer cases also show increases, with the curves within the ranges defined by the lowest and the highest curve in figure 26.

The residual oil saturations at 1-year intervals in the case of lower permeability center layers (layers 4, 5, and 6) for a 40 x 1 x 10 simulation with average k_h = 346.5 md, k_z = 34.6 md is shown in figures 5, 6, and 7. By comparing them to figure 1 (homogeneous 346.5 md), it is clear again that a permeability ratio of 1:2 (Fig. 5) has a neglibile effect on the vertical sweep, whereas high-permeability contrasts of 1:10 (Fig. 6) and 1:100 (Fig. 7) have the effect of trapping the oil in the low-permeability layers and gradually releasing it. As shown in table 7, after similar oil and water production for the first 1½ years, much more water and less oil is being produced by the high-contrast cases than by the low-contrast or homogeneous cases in the following years. The simulation results suggest that when considering the division of the reservoir, layers with permeability contrasts smaller than a factor of 2 can be safely grouped to save on computational time.

The effect of vertical permeability on the ROS distribution at 1-year intervals during waterflooding is shown in figures 8, 9, and 10. Although the ROS distribution varies somewhat with the vertical permeability, it is seen that for k_h/k_z in range 4 to 40, the ROS distribution is affected only slightly. The results of 20 x 1 x 5 simulations for the study of cumulative production versus time for vertical permeability/horizontal permeability ratios 1/1, 1/2, 1/4, 1/10, 1/20, 1/40 are shown in figure 27. The strong effect on lowering the oil recovery is seen for the large vertical permeability values ($k_z = k_h$ to $k_z = k_h/2$). Once the vertical permeability becomes smaller than $k_h/4$, the variation of k_z has a negligible effect on oil recovery (within the simulation error). As seen in figure 28, the number of time steps increases very fast for high vertical permeability as the flow becomes more of the 2D type. The average CPU time per time step was 1.6 seconds.

To study the effect of a shale layer separating the upper and the lower part of the reservoir, simulations were made by considering permeability contrasts between the top and bottom halves in the ratios 1:1, 2:1, 10:1, 100:1 and shale continuity 10, 20, 40, 60, 80 and 100 percent. The shale is simulated by setting to zero the transmissibility between grid blocks in the

layers 5 and 6. Figures 11, 12, and 13 show the ROS distributions at 1-year intervals for the cases with permeability ratios of 2:1 and shale continuity of 10, 40, and 100 percent, respectively. The vertical permeabilities are 1/10 of k_h. As seen, 10 and 40 percent shale have very similar effects. Not shown are the 0 percent and the 80 percent shale which cause similar ROS distribution in figures 11 and 12. The strong effect in the 100 percent shale continuity case is expected, given the fact that it divides the reservoir into two independent flow zones, and the fluids will flow faster in the higher permeability zone when subjected to the same pressure difference. Figures 14 and 15 show the ROS distributions at 1-year intervals for 10 and 40 percent shale and 1:10 permeability contrast between bottom and top layers. The higher permeability contrast (1:10) causes a channeling effect which is enhanced by the presence of the shale.

To study the effect of regressive and transgressive sequences on ROS and oil production, simulations were performed with a 40 x 1 x 5 model with layer permeabilities increasing upward or downward, as shown in table 8. Also shown in table 8 is the number of time steps and CPU time for various cases. Although the CPU time/time step varies only slightly, the number of time steps until WOR = 20 or T = 1825 days almost doubles from case A to case G. The CPU time/time step/grid blocks is in average 1.6×10^{-2} seconds. The larger number of time steps is encountered in the cases of permeability increasing downward in the reservoir and the larger permeability contrasts. The ROS distributions at 1-year intervals are shown in figures 16 through 22 and the cumulative oil production is shown in figure 29. The average permeability was 346.5 md in all cases. The homogeneous case in figure 29 is shown to reach WOR = 20 in about 900 days and has the highest oil production. Although initially the cumulative production curves overlap, figure 24 shows that for the cases of large permeability contrasts, the water breakthroughs occur earlier and the cumulative oil production is lower than in the cases of small permeability contrasts (the water breakthrough takes place where the cumulative oil production curve shows a marked decrease in slope).

As shown in figures 18, 20, 22, and 29, the ROS distribution and cumulative oil production are most severely affected by a transgressive sequence (permeability increasing with depth). In these cases, the gravitational effect is compounded by the high permeability to give an earlier

water breakthrough and a lower production rate afterwards (about 500 days for case C, 900 days for case E, and 300 days for case G). When the permeability increases upward (Figures 17, 19, and 21), the higher permeability of the top layers counterbalances the gravity effect by creating a more vertical waterbank. The production is improved by delaying the water breathrough. Note that the performance for the homogeneous reservoir and the reservoir having a permeability ratio (top to bottom) of 5:1 are nearly identical, whereas their vertical ROS profiles are similar but reversed (upside down).

To be able to predict the expected run time for different numbers of grid blocks, the 2D cross section has been divided into 100, 200, 600, and 800, 1,600 grid blocks. The time step duration versus the number of grid blocks is shown in table 9, which shows essentially a linear relationship with a slope of approximately 1.5×10^{-2} s/time step/grid block. As the size of the grid block decreases, smaller time-steps must be taken to keep the change in pressure and saturation within prescribed limits for each time step.

THREE DIMENSIONAL (3D) WATERFLOOD SIMULATIONS

To study the capability of BOAST to handle high-permeability contrasts, sensitivity studies were performed on a quarter five-spot and two inverted five-spot 3D configurations. ROS distributions for a run containing a shale in layer 3 in a 13 x 7 x 5 grid, (Fig. 30), and with permeabilities decreasing downward (500, 250, 0.1, 50, and 5 md) are shown in figure 31 (after 4 yr) and figure 32 (after 10 yr). The thickness of layers is 10, 10 , 0.5, 10, and 10 ft, and the grid block areal dimensions are $\Delta_x = \Delta y$ = 94.3 ft; vertical permeability for each layer is respectively, 50, 25, 0.1, 5, and 1 md. It is clear that the high-permeability zones are well swept by the end of the waterflood, whereas a significant amount of oil is left in the lower permeability layers situated below the 0.1 md shale layer. The 0.1 md layer is partly swept because of its small height and because it has a large contact area with the 250 md layer situated immediately above it.

3D simulations of the two five-spots have been successfully carried out for 21 x 11 x 10 grid blocks with permeability contrasts between layers ranging from 0.01 to 1,000 md.

DESCRIPTION OF CHEMICAL FLOOD SIMULATOR

Micellar-polymer flooding is attractive as a secondary or tertiary oil recovery process because of its potential for widespread applicability and its technical feasibility; however, a field pilot test for this process is lengthy, and scaling laboratory results to the field is difficult. Consequently, numerical simulation constitutes an integral part of any design or scaleup for a process as complicated as micellar-polymer flooding. By means of numerical simulation, a sensitivity analyses of the process with respect to various variable performance, prediction, and economic analysis can be investigated at relatively low cost. During and after operation of the pilot, the simulation also helps in understanding the behavior of the rock-fluid interactions in the reservoir.

The simulator evaluated in this study was developed at the University of Texas at Austin. The simulator is a three-dimensional, multiphase, multicomponent micellar-polymer flooding simulator. Component number and phase number are defined as follows. At most, nine components are considered: (1) water, (2) oil, (3) surfactant, (4) polymer, (5) total nonsorbing anions, (6) calcium ion, (7) co-surfactant-1, (8) co-surfactant-2, and (9) sodium ion. The maximum number of mobile phases considered is three: (1) aqueous, (2) oleic, and (3) microemulsion. The last one is defined as the phase containing the highest concentration of surfactant.

The major physical phenomena modeled in the simulator are: dispersion, adsorption, interfacial tension, relative permeability, capillary trapping, cation exchange capacity, capillary pressure, phase density, phase behavior, polymer properties, and permeability reduction. A phase-behavior model which can use up to five pseudo-components (brine, oil, surfactant, cosurfactant-1 and cosurfactant-2) is incorporated in the simulator.[38-40]

Model Formulation and Solution Procedure

The basic equations describing isothermal, multicomponent, multiphase flow in permeable media are the species conservation equations and an overall mass continuity equation. The continuity equation combined with Darcy's law yields the pressure equation. The governing equations are the pressure equation together with (n-1) material conservation equations in the form of an initial-boundary value system of partial differential equations.

The assumptions made in the mathematical formulation are: (1) a isothermal reservoir; (2) incompressible fluid and rock properties; (3) no precipitation or chemical reaction; (4) local thermodynamic equilibrium exists; (5) Darcy's law applies for non-Newtonian flow (apparent viscosity is used in Darcy's equation); (6) dispersion follows a generalization of Fick's law to multiphase flow in porous media; and (7) ideal mixing holds (volume change of mixing is zero).

A finite-difference approximation is used to convert the partial differential basic equations to linear equations. A block centered grid has been used in the formulation. The solution scheme for the governing linear equations follows a two-step procedure. First, the pressure equation is solved for implicitly using explicit dating of saturation dependent terms, then the total concentrations are calculated explicitly (the procedure is similar to IMPES).

Limitations of Available Version of Micellar-Polymer Simulator

The version of the micellar-polymer simulator available at NIPER cannot handle (1) variable grid size, (2) variable initial water saturation, (3) fluid compressibility, (4) variable rock type, (5) dispersion control, or (6) more than one surfactant system.

After NIPER acquired the program, work at the University of Texas has continued to improve the program, and at present, their program allows (1) fluid compressibility, (2) variable grid size, (3) variable initial water saturation, (4) dispersion control in three dimensions, and (5) the use of three additional tracer components.

It is anticipated that this version of the simulator can be obtained from the University of Texas whenever required for future work in the reservoir characterization project. As stated above the present simulator cannot handle variable rock type or more than one surfactant system. This implies that for a heterogeneous reservoir (more than one type of rock present) only a single set of values for rock-fluid properties (polymer and surfactant adsorption, relative permeability, capillary trapping, dispersion parameters, etc.) can be input to the simulator. Modification of the simulator will be required to simulate different rock types in a heterogeneous reservoir. The computer time required to simulate the micellar-polymer process in a heterogeneous reservoir

must be considered even more than for of waterflood simulations. At present, a 2- to 3-year simulation of a homogeneous reservoir using 2,800 grid blocks requires about 1,000 sec of computing time with a Cray computer.

The available simulator is capable of handling variable permeability, variable porosity, and variable pore volume. Also grid block transmissibilities can be easily changed so that other heterogeneities (such as shale streaks) can be easily simulated.

SUMMARY AND CONCLUSIONS

Based on the results of the simulations performed, we have made the following conclusions:

1. The graphical display of residual oil saturations developed at NIPER is an essential tool for studying how various heterogeneities affect the displacement of oil from a reservoir.

2. BOAST handles adequately the range of permeability variations and contrasts typical for the depositional system studied in the geoscience base programs.

3. The effect of oil trapping in low permeability layers and oil and water channeling in high-permeability layers is shown both in the residual oil distribution graphical displays and in the cumulative oil production curves.The presence of a thin (less than one-third of reservoir thickness) high- or low-permeability layer in a reservoir does not have a significant effect on the oil recovery unless the permeability ratio between it and the rest of the reservoir is larger than 2.

4. The effect of variation in vertical permeability on oil saturation and oil production is highly significant for k_h/k_z ratios smaller than 4. Once the ratio becomes greater than 4, its variation affects only very slightly the oil production (essentially the reservoir presents more of a 1D flow for a 2D reservoir model or a 2D flow for a 3D reservoir model).

5. Shale layers have a strong effect on residual oil saturation distribution (for $k_z = k_h/10$) only if they are essentially continuous. When a continuous shale layer separates two zones of different permeabilities, even a small permeability contrast (permeability ratio = 2) between the two zones can have a marked effect on the ROS in both zones.

6. The higher the permeability contrasts between the layers, the earlier the water breakthrough takes place and the lower the cumulative oil production. The gradual vertical variations in permeability compound the effect of gravity in producing an earlier water breakthrough when the higher permeability is at the bottom of the reservoir. The vertical variation in permeability counteracts the action of gravity when the higher permeability is at the top of the reservoir. Thus a permeability ratio of 5 between top and bottom layers and a permeability ratio of 1 (homogeneous case) give mirror image ROS distributions and almost identical oil production curves. For smaller ratios, with higher top permeability, the oil displacement is more pistonlike, which is a desirable effect.

7. The computation time increases as the vertical permeability increases and as the permeability contrast between layers is increased. Models with 2,000 grid blocks and moderate heterogeneity are expected to require CPU times on the Microvax in the 10 to 20 h range.

8. The simulator should be adapted to accept different relative permeability and capillary pressure curves for different layers as it is expected that different types of reservoir rock will have different absolute permeabilities, relative permeabilities, and capillary pressures. Sensitivity studies for variations in relative permeability should also be performed.

9. At present, the productivity index (PID), is determined empirically from history matching and well tests. Since it has a very strong effect on the oil production from a given well, it is important to have the PID value determined accurately for actual field studies. The formula for the initial PID value given in the BOAST manual gives only the initial estimate of the PID.

10. Simulation runs of reservoirs containing the heterogeneities studied in this report should also be performed with other simulators, such as adaptive implicit simulators.

11. Simulation runs on small heterogeneity models should be performed on the improved Chem 3D model when it becomes available.

REFERENCES

1. Suder, F. E. An Engineering Study of Water Flooding the Burkett Oil Field, Greenwood County, Kansas. M.S. Thesis. Univ. of Oklahoma, 1948.

2. Stiles, W. E. Use of Permeability Distribution in Waterflood Calculations. Trans., AIME, v. 186, January 1949, pp. 9-13.

3. Muskat, M. The Effect of Permeability Stratification in Complete Water Drive Systems. Trans., AIME, v. 189, December 1950, pp. 349-358.

4. Schmaltz, T. P. and M. S. Rahme. The Variation in Waterflood Performance with Variation in Permeability Profile. Prod. Monthly, v. 15, No. 9, 1950 pp. 9-12.

5. Dykstra, M. and R. L. Parsons. The Prediction of Oil Recovery by Waterflood. Secondary Recovery of Oil in the United States, 2nd Ed. API, 1950, pp. 160-170.

6. Neil, S. D., M. L. Chang, and T. M. Geffen. Improved Oil Recovery. Interstate Oil Compact Commission, 1983, pp. 1-67.

7. Koval, E. J. A Method for Predicting the Performance of Unstable Miscible Displacement in Heterogeneous Media. SPEJ, June 1963, pp. 145-154.

8. Jensen, J. L. and L. W. Lake. The Influence of Sample Size and Permeability Distribution Upon Heterogeneity Measures. Pres. at Soc. Petrol. Eng. 61st Ann. Tech. Conf. and Exhib., New Orleans, LA, Oct. 5-8, 1986. SPE paper 15434.

9. Warren, J. E. and H. S. Price. Flow in Heterogeneous Porous Media. SPEJ, v. 1, No. 3, September 1961, pp. 153-169.

10. Warren, J. E. and F. F. Skiba. Macroscopic Dispersion. SPEJ, v. 4, No. 3, September 1964, pp. 215-229.

11. Warren, J. E., and J. J. Cosgrove. Prediction of Waterflood Behavior in a Stratified System. SPEJ, v. 4, No. 2, June 1964, p. 149.

12. Huppler, J. D. Numerical Investigation of the Effects of Core Heterogeneities on Waterflood Relative Permeabilities. SPEJ, v. 10, No. 4, December 1970, pp. 381-392.

13. Hearn, C. C. Simulation of Stratified Waterflooding by Pseudo Relative Permeability Curves. J. Pet. Tech., v. 23, July 1971, pp. 805-813.

14. Hawthorne, R. G. A Model of Fluid Displacement in Multilayer Porous Media Including Capillary Pressure Effects Between Layers. Pres. at Soc. Petrol. Eng. 49th Ann. Meeting, Houston, TX. Oct. 6-9, 1974. SPE paper 5126.

15. Jacks, H. H., O. J. Smith, and C. C. Mattox. The Modeling of a 3-D Reservoir With a 2-D Reservoir Simulator. The Use of Dynamic Pseudo Functions. SPEJ, v. 13, No. 3, June 1973, pp. 175-185.

16. Kyte, J. R., and D. W. Berry. New Pseudo Functions to Control Numerical Dispersion. Pres. at Soc. Petrol. Eng. 49th Ann. Fall Meeting, Houston, TX, 1974; SPEJ, v. 15, No. 4, 1975, pp. 269-276.

17. Kortekaas, T. F. M. Water/Oil Displacement Characteristics in Cross Bedded Reservoir Zones. Pres. at Soc. Petrol. Eng. 58th Ann. Tech. Conf. and Exib., San Francisco; SPEJ, v. 15, No. 6, December 1985, pp. 917-926.

18. Lake, L. W. and G. J. Hirasaki. Taylor's Dispersion in Stratified Porous Media. Pres. at Soc. Petrol. Engr. 54th Ann. Tech. Conf. and Exib., Las Vegas, NV., Sept. 23-26, 1976. SPE paper 8436.

19. Haldorsen, H. H. and L. W. Lake. A New Approach to Shale Management in Field Scale Simulation Models. Pres. at Soc. Petrol. Eng. 57th Ann. Fall Tech. Conf. and Exhib. New Orleans, LA, September 1982. SPE paper 10976.

20. Zeito, G. A. Interbedding of Shale Breaks and Reservoir Heterogeneities. J. Pet. Tech., v. 17, No. 10, October 1965, pp. 1223-1228.

21. Martin, T. H. and T. A. Cooper. An Intergrated Approach to the Modeling of Permeability Barrier Distribution in a Sedimentologically Complex Reservoir. Pres. at Soc. Petrol. Engr. 59th Ann. Tech. Conf. and Exhib., Houston TX, Sept. 16-19, 1984. SPE paper 13051.

22. Begg, S. H. and P. R. King. Modeling the Effects of Shales on Reservoir Performance: Calculation of Effective Vertical Permeability. Pres. at 8th Soc. Petrol. Eng. Symp. on Reservoir Simulation, Dallas, TX, Feb. 10-13, 1985. SPE paper 13529.

23. Haldorsen, H. H. and D. M. Chang. Notes on Stochastic Shales: From Outcrop to Simulation Model. In Reservoir Characterization. Eds. L. W. Lake, and H. B. Carroll, Academic Press, 1986, p. 665.

24. Begg, S. H., D. M. Chang, and H. H. Haldorsen. A Simple Statistical Method for Calculating the Effective Vertical Permeability of a Reservoir Containing Discontinuous Shales. Pres. at Soc. of Petrol. Eng. 60th Ann. Tech. Conf. and Exhib., Las Vegas, NV, September 1985. SPE paper 14271.

25. Davies, B. J. and H. H. Haldorsen. Pseudofunctions in Formations Containing Discontinuous Shales: A Numerical Study. Pres. at Soc. Petrol. Eng. 9th Symp. on Reservoir Simulation, San Antonio, TX, February 1987, Proceedings pp. 221-230. SPE paper 16012.

26. White, C. D. and R. N. Horne. Computing Absolute Transmissibility in the Presence of Fine Scale Metering. Pres. at Soc. of Petr. Eng. 9th Symp. on Reservior Simulation, Feb. 1-6, 1987, Proceedings pp. 209-220. SPE paper 16011.

27. Shaw, D. C., and R. A. Dawe. Averaging Laws for Flow Through Grid Blocks Containing Heterogeneities. Pres. at Soc. of Petrol. Eng. 8th Symp. on Reservoir Simulation, Dallas, TX, Feb. 10-13, 1985. SPE paper 13530.

28. Leung, W. F. A Tensor Model for Anisotropic and Heterogeneous Reservoirs with Variable Directional Permeability. Pres. at Soc. of Petrol. Eng. 56th Calif. Regional Meeting, Oakland, CA, Apr. 2-6, 1986. SPE paper 15134.

29. Lasseter, T. J., T. R. Waggoner and L. W. Lake. Reservoir Heterogeneities and Their Influence on Ultimate Recovery. In Reservoir Characterization. Eds., L. W. Lake and H. B. Carroll, Academic Press, 1986, pp. 545-560.

30. Poston S. W., S. J. Gross. Numerical Simulation of Sandstone Reservoir Models. SPE Reservoir Engineering v. 1, July 1986. pp. 423-429.

31. Arya, A., T. A. Hewett, R. Larson, and L. W. Lake. Dispersion and Reservoir Heterogeneities. Pres. at Soc. of Petrol. Eng. 60th Ann. Tech. Conf. and Exhib., Las Vegas, NV, September 1985. SPE paper 14364.

32. Dawe, R. A., M. R. Wheat and R. J. Wright. Effects of Heterogeneities on Miscible Flow Processes in EOR. Pres. at 3rd European Meeting on Improved Oil Recovery, Rome, Apr. 16-18, 1985, Proceedings pp. 99-109.

33. Wheat, M. R. and R. A. Dawe. Transverse Dispersion in Slug Mode Chemical EOR Processes in Stratified Porous Media. Pres. at 5th SPE/DOE Symp. on Enhanced Oil Recovery, Tulsa, OK, Apr. 20-23, 1986. SPE/DOE paper 14890.

34. Novosad, J. The Effect of Rock Heterogeneity and Wettability on Chemical Flooding. Pres. at 3rd European Meeting on Improved Oil Recovery, Rome, Apr. 16-18, 1985, Proceedings pp. 145-153.

35. King, M. J. and M. Scher. Probabilistic Stability Analysis of Multiphase Flow in Porous Media. Pres. at Soc. of Petrol. Eng. 60th Ann. Tech. Conf. and Exhib., Las Vegas, NV, September 1985. SPE paper 14366.

36. Datta, Gupta, A. G. A. Pope and J. K. Sepehrnoori. Effects of Reservoir Heterogeneity on Chemically Enhanced Oil Recovery. Pres. at 5th SPE/DOE Symp. on Enhanced Oil Recovery, Tulsa, OK, April 2023, 1986. SPE/DOE paper 14889.

37. Fanchi, T. R. Harpole, K. J and S. W. Bujnowski. BOAST: A Three-Dimensional, Three-Phase Black Oil Applied Simulation Tool (Version 1.1). Vol. I: Technical Description and Fortran Code, Dept. of Energy Report DOE/BC/1033-3, 1982. NTIS Order No. DE83000529; v. 2: Program User's Manual, Dept. of Energy Report No. DOE/BC/1033, 1982. NTIS Order No. DE83003031.

38. Datta-Gupta, Akhil. Three Dimensional Simulation of Chemical Flooding. M.S. Thesis, Univ. of Texas, Austin, May 1985.

39. Prouvost, L. P., T. Satoh, K. Sepehrnoori, G. A. Pope. A New Micellar Phase-Behavior Model for Simulation Systems With Up To Three Amphiphilic Species. Pres. at Soc. Petrol. Eng. 59th Ann. Tech. Conf. and exhib., Houston, TX, Sept. 16-19, 1984. SPE paper 13031.

40. Satoh, T. Treatment of Phase Behavior and Associated Properties Used in Micellar/Polymer Flood Simulator. M.S. Thesis, Univ. of Texas, Austin, 1984.

TABLE 1. - Empirical data

SAT	KRO	KRW	KRG	PCOW	PCGO
0.1000	0.0000	0.0000	0.0000	0.00	0.00
0.2000	0.0000	0.0000	0.0000	0.00	0.00
0.1000	0.0000	0.0000	0.0250	0.00	0.00
0.2000	0.0000	0.0000	0.0750	0.00	0.00
0.3000	0.0000	0.0122	0.1900	0.00	0.00
0.4000	0.0300	0.0244	0.4100	0.00	0.00
0.5000	0.0900	0.0366	0.7200	0.00	0.00
0.6000	0.1700	0.0672	0.8700	0.00	0.00
0.7000	0.3000	0.1344	0.9400	0.00	0.00
0.8000	0.5000	0.2688	0.9667	0.00	0.00
0.9000	0.7500	0.4704	0.9933	0.00	0.00
1.0000	1.0000	0.5000	1.0000	0.00	0 00

PBO (PSIA)	MUSLOPE (CP/PSI)	BSLOPE (RB/STB/PSI)	RSLOPE (SCF/STB/PSI)	PMAX (PSIA)	IREPRS
4014.70	0.460E-04	-0.232E-04	0.00	9014.70	0

P (PSIA)	MUO (CP)	BO (RB/STB)	RSO (SCF/STB)
14.7	1.0400	1.0620	1.00
1014.7	0.8300	1.2950	371.00
2014.7	0.6950	1.4350	636.00
3014.7	0.5940	1.5650	930.00
4014.7	0.5100	1.6950	1270.00
5014.7	0.4490	1.3270	1270.00

P (PSIA)	MUW (CP)	BW (RB/STB)	RSW (SCF/STB)
14.7	0.5000	1.0190	0.00
1014.7	0.5010	1.0160	0.00
2014.7	0.5020	1.0130	0.00
4014.7	0.5050	1.0070	0.00
6014.7	0.5100	1.0010	0.00

P (PSIA)	MUG (CP)	BG (RCF/SCF)	CR (1/PSI)
14.7	0.0080	0.9358E+00	0.300E-05
264.7	0.0096	0.6790E-01	0.300E-05
514.7	0.0112	0.3523E-01	0.300E-05
1014.7	0.0140	0.1795E-01	0.300E-05
2014.7	0.0189	0.9063E-02	0.300E-05
2514.7	0.0208	0.7266E-02	0.300E-05
3014.7	0.0228	0.6064E-02	0.300E-05
4014.7	0.0268	0.4554E-02	0.300E-05
5014.7	0.0309	0.3644E-02	0.300E-05
9014.7	0.0470	0.2167E-02	0.300E-05

RHOSCO (LB/CU.FT.)	RHOSCW (LB/CU.FT.)	RHOSCG (LB/CU.FT.)
46.2440	62.2380	0.0647

TABLE 2. - Slopes for compressibility calculations

A. Oil

P (PSIA)	BO (RB/STB)	DBO/DP (RB/STB/PSIG)	RSO (SCF/STB)	DRSO/DP (SCF/STB/PSI)
1014.7	1.2950	0.2330E-03	66.1	0.6589E-01
2014.7	1.4350	0.1400E-03	113.3	0.4719E-01
3014.7	1.5650	0.1300E-03	165.6	0.5236E-01
4014.7	1.6950	0.1300E-03	226.2	0.6055E-01
5014.7	1.8270	0.1320E-03	288.1	0.6198E-01

B. Water

P (PSIA)	BW (RB/STB)	DBW/DP (RB/STB/PSI)	RSW (SCF/STB)	DRSW/DP (SCF/STB/PSI)
1014.7	1.0160	-0.3000E-05	0.0	0.0000E+00
2014.7	1.0130	-0.3000E-05	0.0	0.0000E+00
4014.7	1.0070	-0.3000E-05	0.0	0.0000E+00
6014.7	1.0010	-0.3000E-05	0.0	0.0000E+00

C. Gas

P (PSIA)	BG (RCF/SCF)	DBG/DP (RCF/SCF/PSI)
264.7	0.6790E-01	-0.3472E-02
514.7	0.3523E-01	-0.1307E-03
1014.7	0.1795E-01	-0.3455E-04
2014.7	0.9063E-02	-0.8888E-05
2514.7	0.7266E-02	-0.3594E-05
3014.7	0.6064E-02	-0.2404E-05
4014.7	0.4554E-02	-0.1510E-05
5014.7	0.3644E-02	-0.9100E-06

TABLE 3. - Run control parameters

Maximum Number of Time-Steps = 3000			
Factor for Increasing Delt = 1.200000	When DSMAX and DPMAX not exceeded.		
Factor for Decreasing Delt = 0.500000	When DSMAX or DPMAX is exceeded.		
Maximum Simulation Time = 1825.000000			
Maximum Reservoir WOR/Time-Step = 20. STB/STB			
Maximum Reservoir GOR/Time-Step = 500000. SCF/STB			
Minimum Average Reservoir Pressure/Time-Step = 150.			
Maximum Average Reservoir Pressure/Time-Step = 10000.			
Solution Method is LSOR:			
Maximum Number of Iterations	(MITR)	=	3000
Initial Acceleration Parameter	(OMEGA)	=	1.7000
Maximum Pressure Residual	(TOL)	=	0.1000
Parameter for Changing Omega	(TOL1)	=	0.0000
Automatic Time Step Criteria:			
Maximum Allowed Saturation Change	(DSMAX)	=	0.0500
Maximum Allowed Pressure Change	(DPMAX)	=	100.0000

TABLE 4

A. Code for ROS distribution displays (Figs. 3 and 6)

Color	ROS ranges
Light green	ROS ≤ 0.345
Dark green	(0.345 - 0.395]
Light red	(0.395 - 0.445]
Dark red	(0.445 - 0.495]
Light blue	(0.495 - 0.545]
Dark blue	(0.545 - 0.595]
Light purple	(0.595 - 0.645]
Dark purple	(0.645 - 0.695]
Grey	(0.695 - 0.745]
Black	0.745 <ROS

B. Pattern code for ROS distributions

for black and white displays (Figs. 1, 2, 4, 5, 7-22)

ROS<0.45, [0.45,0.5] (0.5,0.55] (0.55,0.6] (0.6,0.65] (0.65,0.7] 0.7<ROS

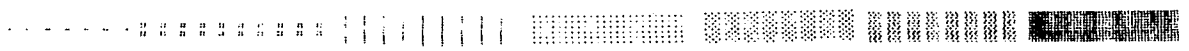

Table 5. - Code for ROS differences

Code	$\Delta ROS = ROS_{homog} - ROS_{heterog}$
Black	<-0.45
Grey	[-0.45,-0.4)
Violet	[-0.4,-0.35)
Light violet	[-.35,-0.3)
Blue	[-.3,-0.25)
Light blue	[-.25,-0.2)
Magenta	[-.2,-0.15)
Light magenta	[-.15,-0.1)
Yellow	[-.01,-0.05)
Light yellow	[-0.05,-0.)
Light orange	[0,0.05)
Orange	[0.05,.1)
Light green	[0.1,0.15)
Green	[0.15,0.2)

TABLE 6. - High permeability center layers cases

Time, yrs	Cum. water production, STB				Cum. oil production, 10^5 STB				WOR			
Perm. ratios	1:1	1:2	1:10	1:100	1.1	1:2	1:10	1:100	1:1	1:2	1:10	1:100
0.5	4.4	4.15	3.78	3.9	0.127	0.122	0.113	0.113	0	0	0	0
1	7.82	7.15	5.98		0.224	0.218	0.21		0	0	0	>20
1.5	11.2	9.96	2800		0.324	0.311	0.29		0	0	1.45	
2	27	12.5	11800		0.428	0.413	0.335		0.025	0	2.52	
2.5	4960	5690	22500		0.496	0.476	0.368		3.38	6.46	3.96	
3			34900				0.394		>20	>20	5.67	
3.5			47500				.411				8.3	
											>20	

TABLE 7. - Low permeability center layers cases

Time, yr	Cum. water prod., STB				Cum. oil production, 10^5 STB				WOR			
Perm Ratios	1:1	1:2	1:10	1:100	1:1	1:2	1:10	1:10	1:1	1:2	1:10	1:100
0.5	4	4	4	4	0.127	0.124	0.120	0.120	0.0	0.0	0.0	0.0
1	8	7	7	7	0.224	0.218	0.218	0.223	0.0	0.0	0.0	0.0
1.5	11	11	10	14	0.324	0.314	0.320	0.327	0.0	0.0	0.0	0.021
2	27	259	3460	9240	0.428	0.416	0.400	0.370	.025	0.23	1.23	12.6
2.5	4400	5550	13600	22960	0.496	0.483	0.429	0.379	3.38	1.59	6.18	15.5
3		17800	25100	36410		0.496	0.444	0.386	>20	>20	8.15	18.7
3.5			37500	50250			0.456	0.393			12.8	>20
4			50600	63220			0.466	0.398			13.7	>20
4.5			63200	76230			0.473	0.403			17.5	33.2
5			76300	90290			0.480	0.407			24.8	32.5

TABLE 8. - Regressive and transgressive sequences simulations

Case	k_{top} / k_{bottom}	Layer permeabilities, md					Simulation duration, days (until WOR=20 or time= 1825days)	Number of time steps	CPU Time (Microvax) (minutes)	CPU Time/ time step, (seconds)
		1(top)	2	3	4	5(bottom)				
	1	346.5	345.5	346.5	345.5	346.5	952	641	34	3.2
B	5	667.5	443.1	296.3	198.1	132.5	1094	676	37	3.3
C	0.2	132.5	198.1	296.3	443.1	662.5	1370	998	53	3.2
D	25	975.1	436.1	195.0	87.2	39	1630	946	56	3.5
E	0.04	39.0	87.2	195.0	436.1	975.1	1825	1323	75	3.4
F	100	1188.4	375.8	118.8	37.6	11.9	1630	1026	60	3.5
G	0.01	11.9	37.6	118.8	375.8	1188.4	1825	1542	80	3.1

TABLE 9. - Run time studies

Number of grid blocks	Time step duration (CPU seconds)	Number time steps for 2.5 yr run
100 (20x1x5)	1.7	308
200 (20x1x10)	3.2	593
400 (40x1x10)	6.5	793
800 (80x1x10)	12.3	1288
1600 (80x1x20)	24.4	2317

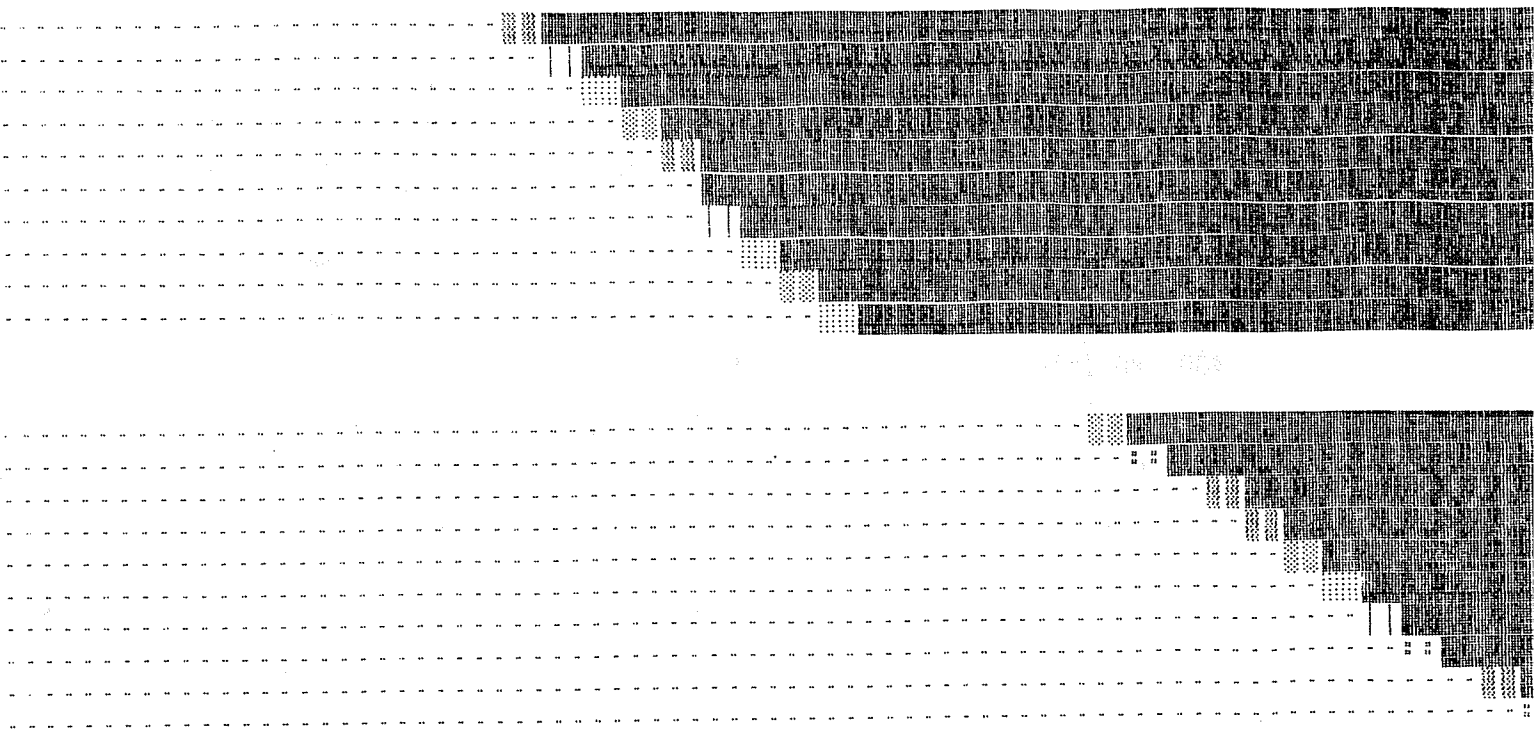

FIGURE 1. - ROS distribution 2D (k_h = 346.5 md).

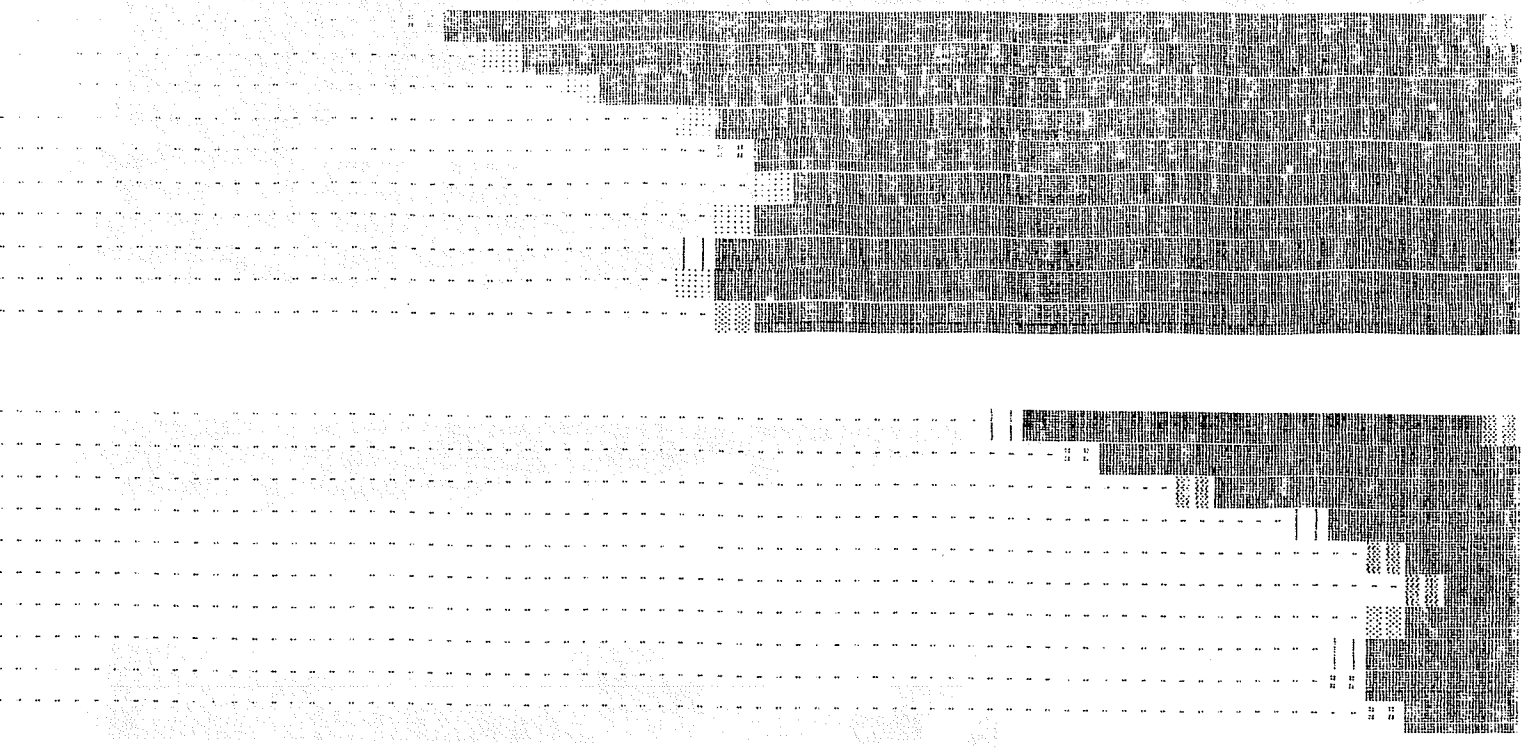

FIGURE 2. - ROS Distribution 2D (k_h = 265 md layer 1,2,3,7,8,9,10, K_h = 533 md layer 4,5,6).

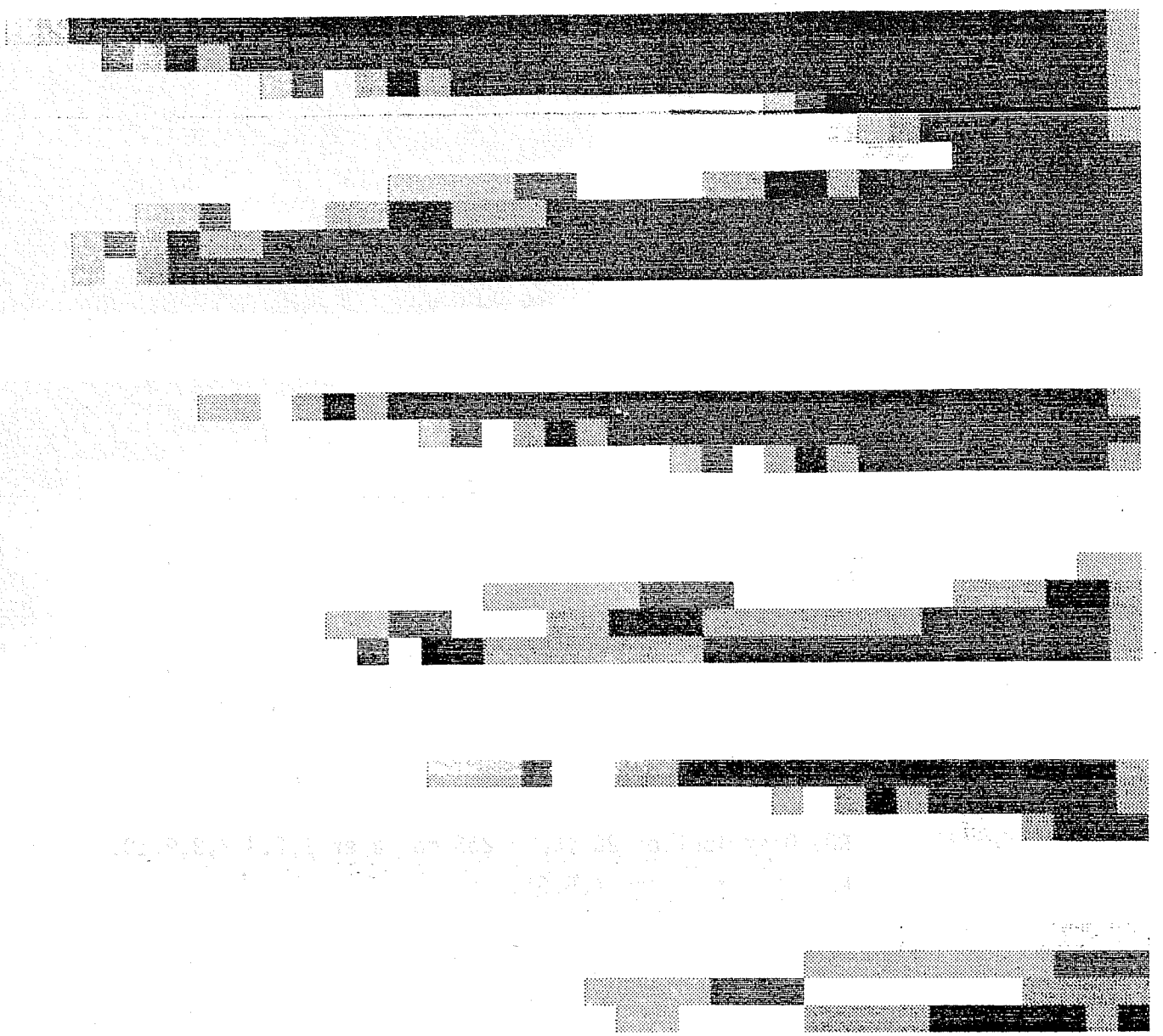

FIGURE 3. - ROS Distribution 2D (k_h = 93.6 md layer 1,2,3,7,8,9,10, k_h = 939 md layer 4,5,6).

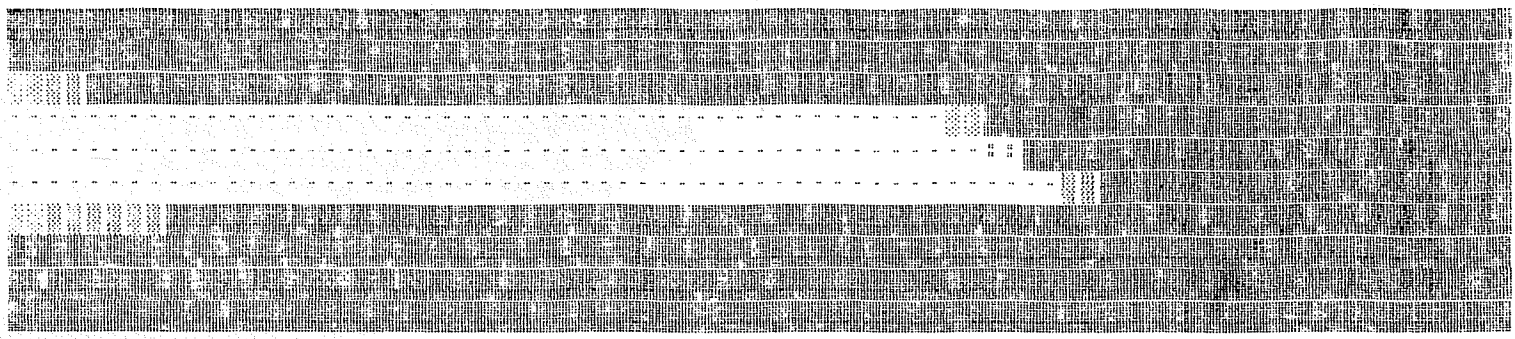

FIGURE 4. - ROS Distribution 2D (k_h = 11.3 md layer 1,2,3,7,8,9,10, k_h = 1129 md layer 4,5,6).

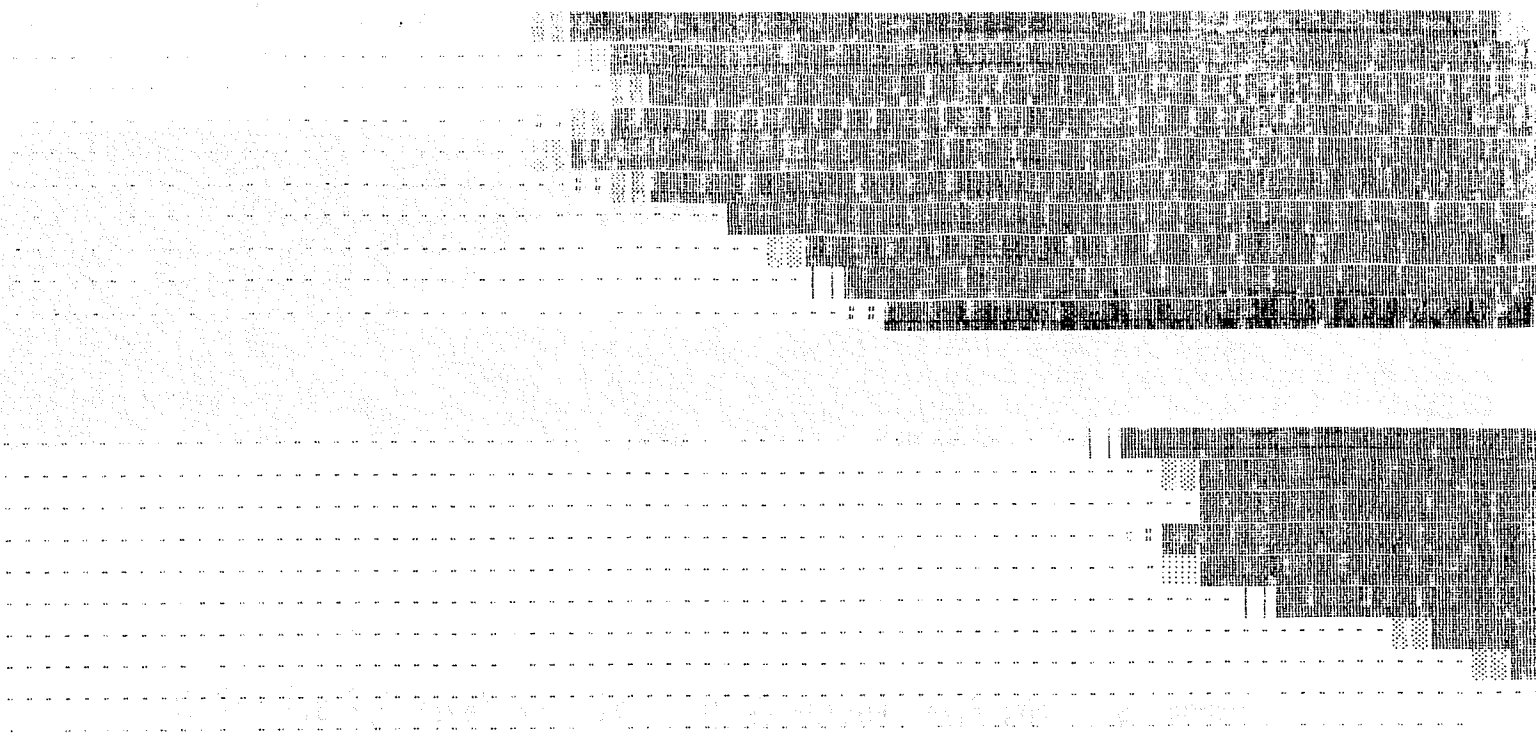

FIGURE 5. - ROS Distribution 2D (k_h = 407 md layer 1,2,3,7,8,9,10, k_h = 203 md layer 4,5,6).

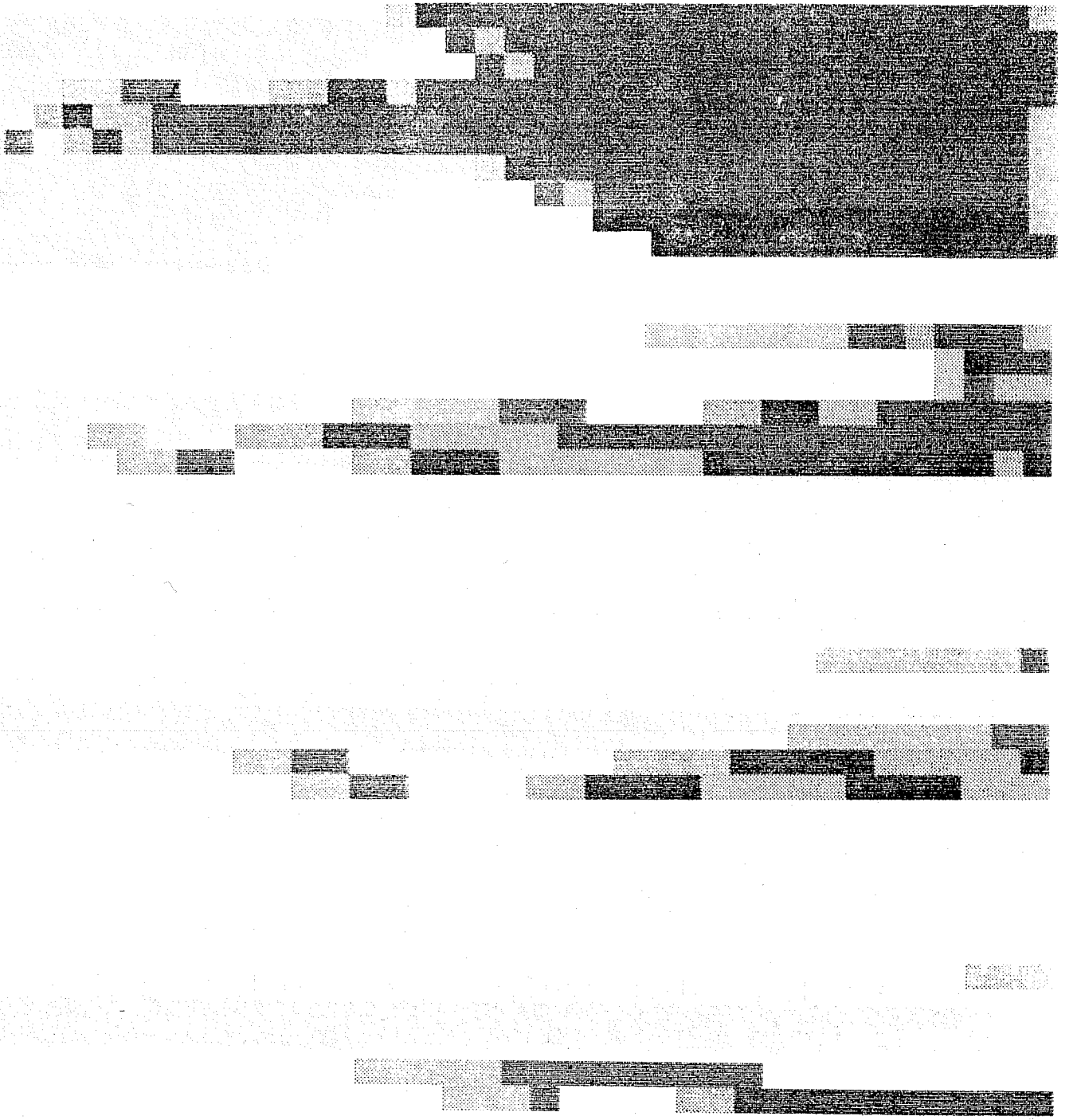

FIGURE 6. - ROS Distribution 2D (k_h = 474 md layer 1,2,3,7,8,9,10, k_h = 47.5 md layer 4,5,6).

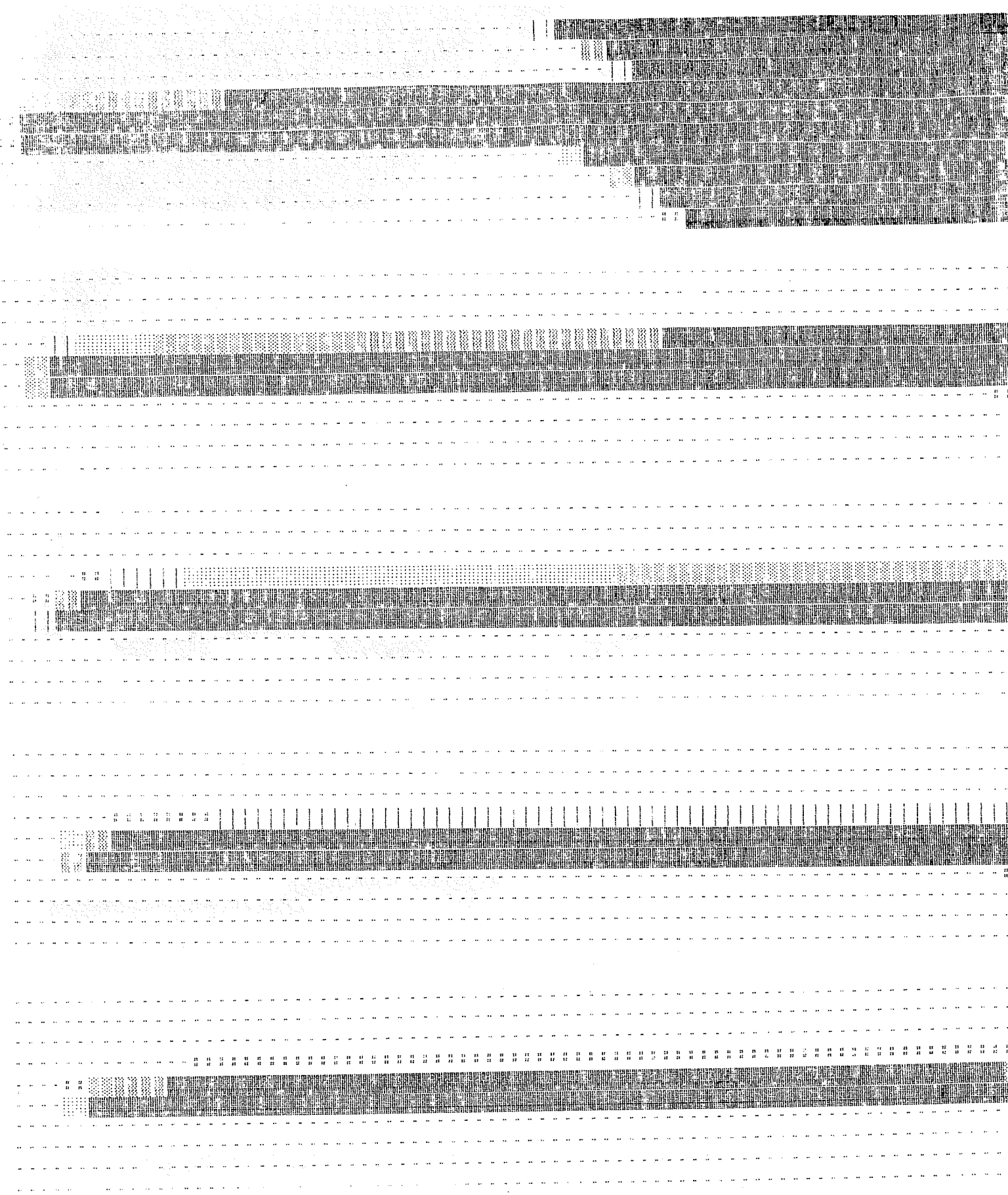

FIGURE 7. - ROS Distribution 2D (k_h = 492 md 1,2,3,7,8,9,10', k_h = 4.92 md layer 4,5,6).

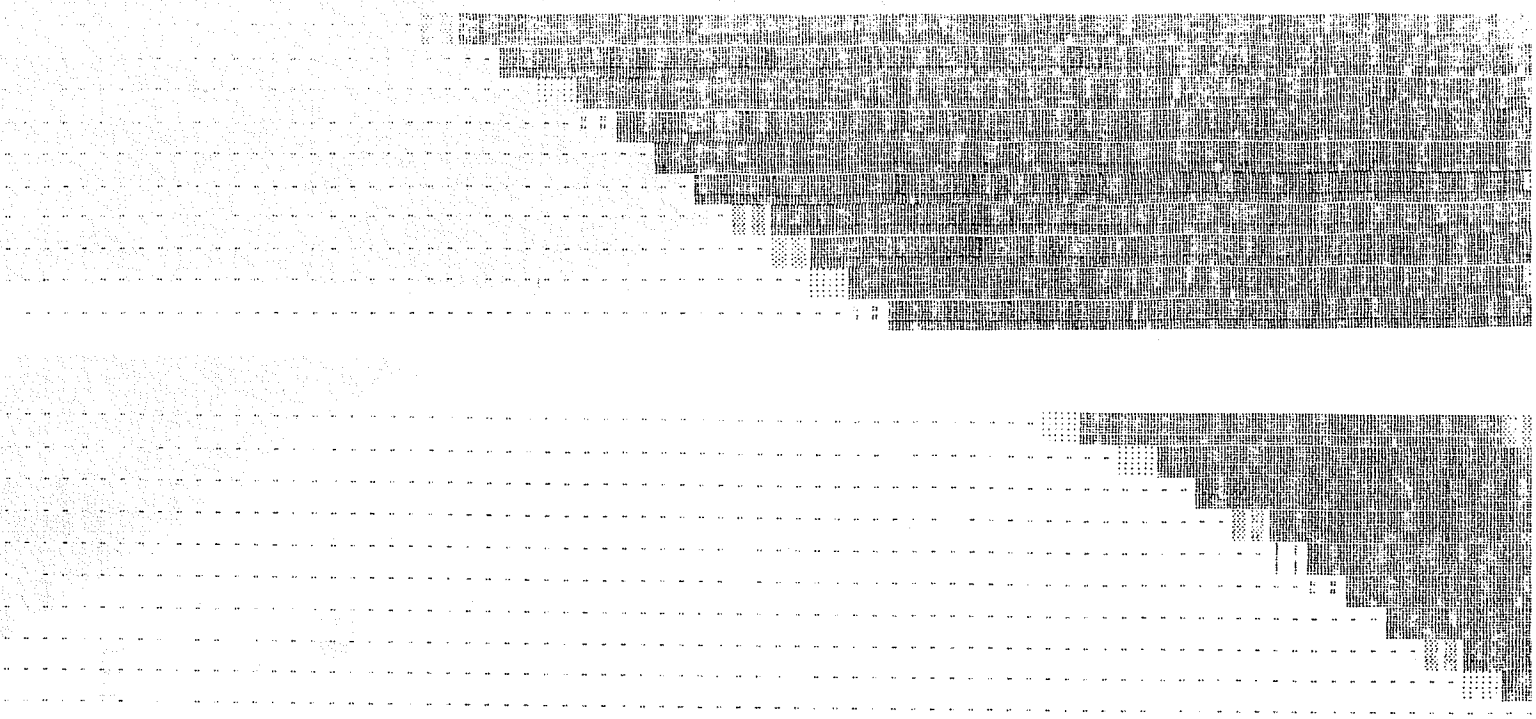

FIGURE 8. - ROS Distribution 2D (k_h/k_z = 1, k_h = 346.5 md).

FIGURE 9. - ROS Distribution 2D (k_h/k_z = 5, k_h = 346.5 md).

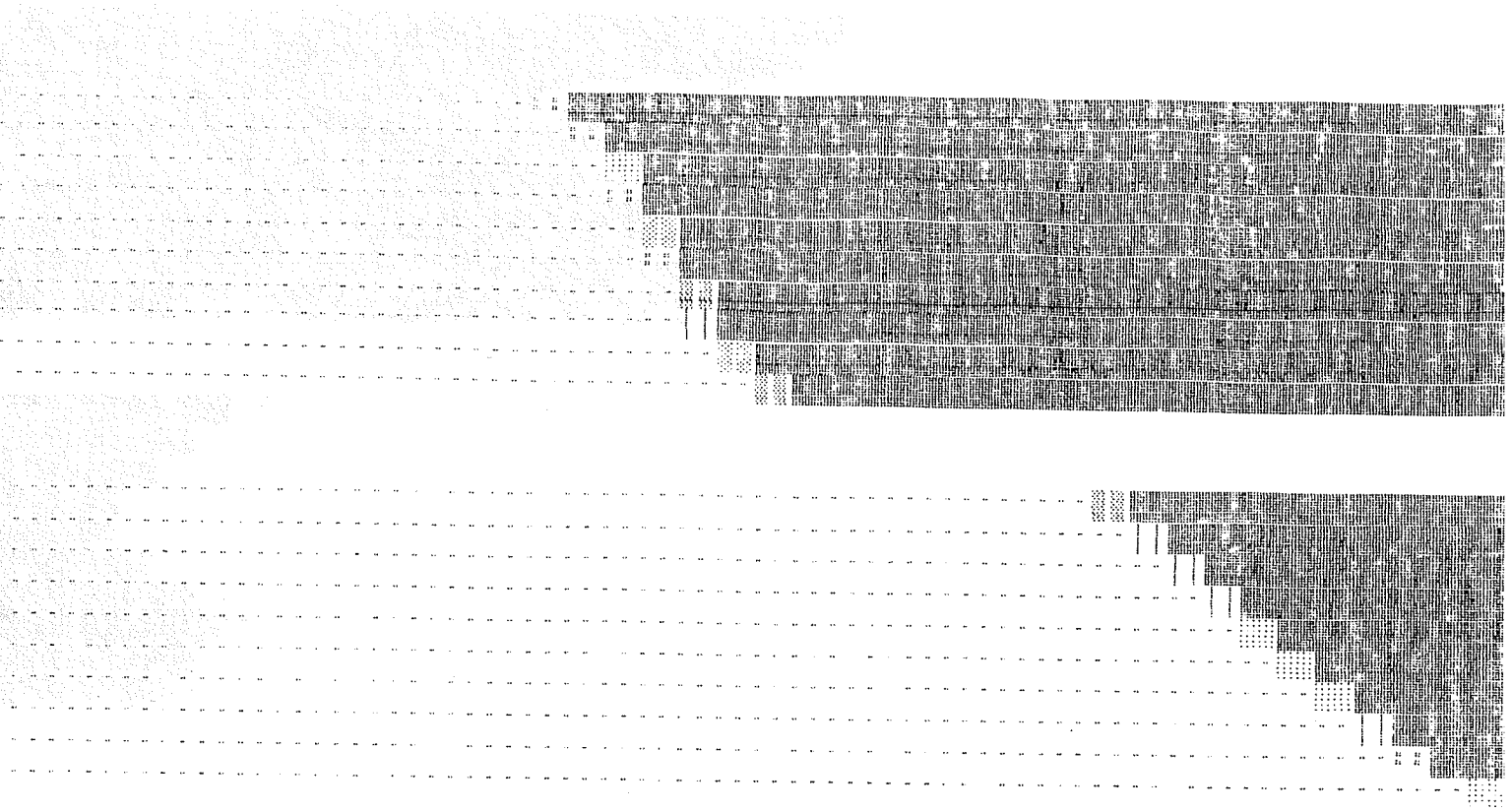

FIGURE 10. - ROS Distribution 2D (k_h/k_z = 40, k_h = 346.5 md).

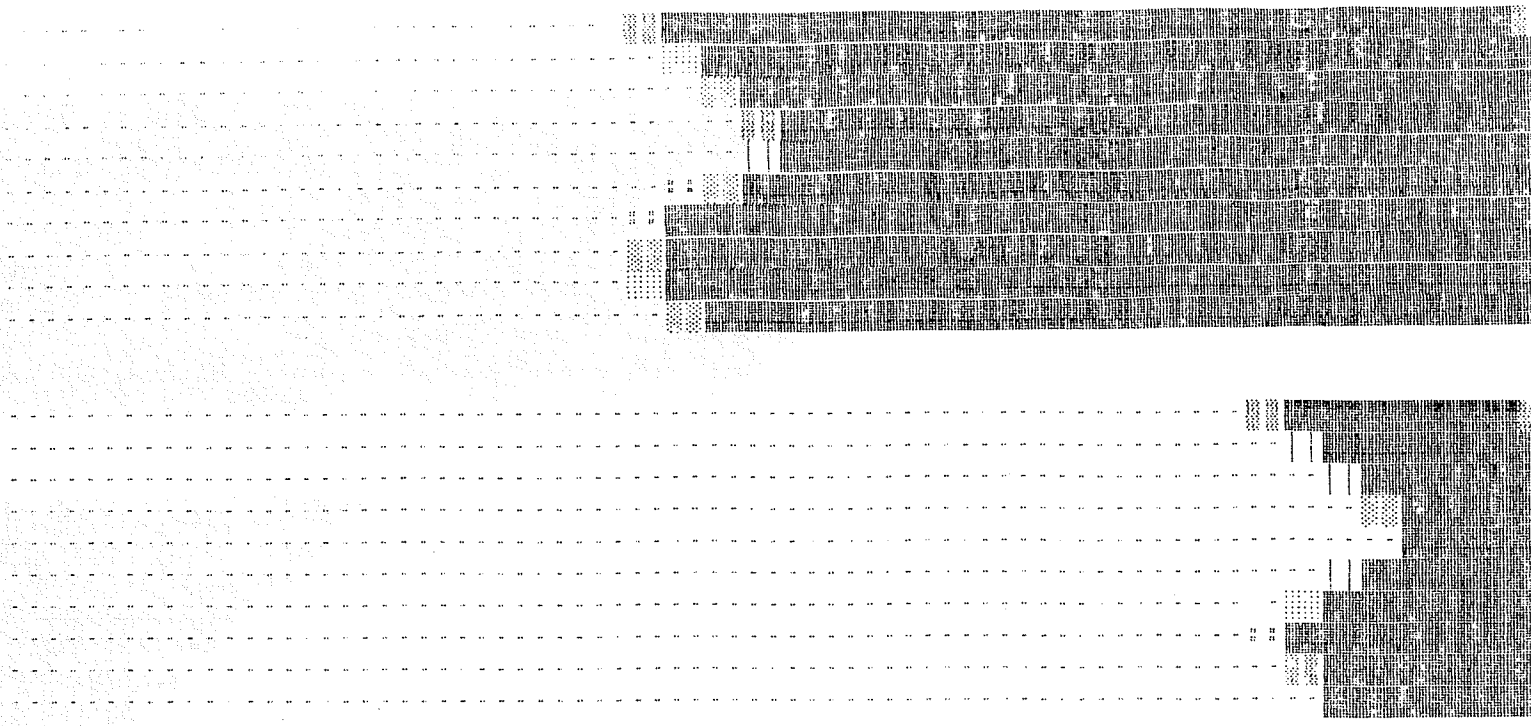

FIGURE 11. - ROS Distribution 2D (k_h = 462 md layer 1,4,5, k_h = 231 md layer 6-10, 10% shale between layer 5 and 6).

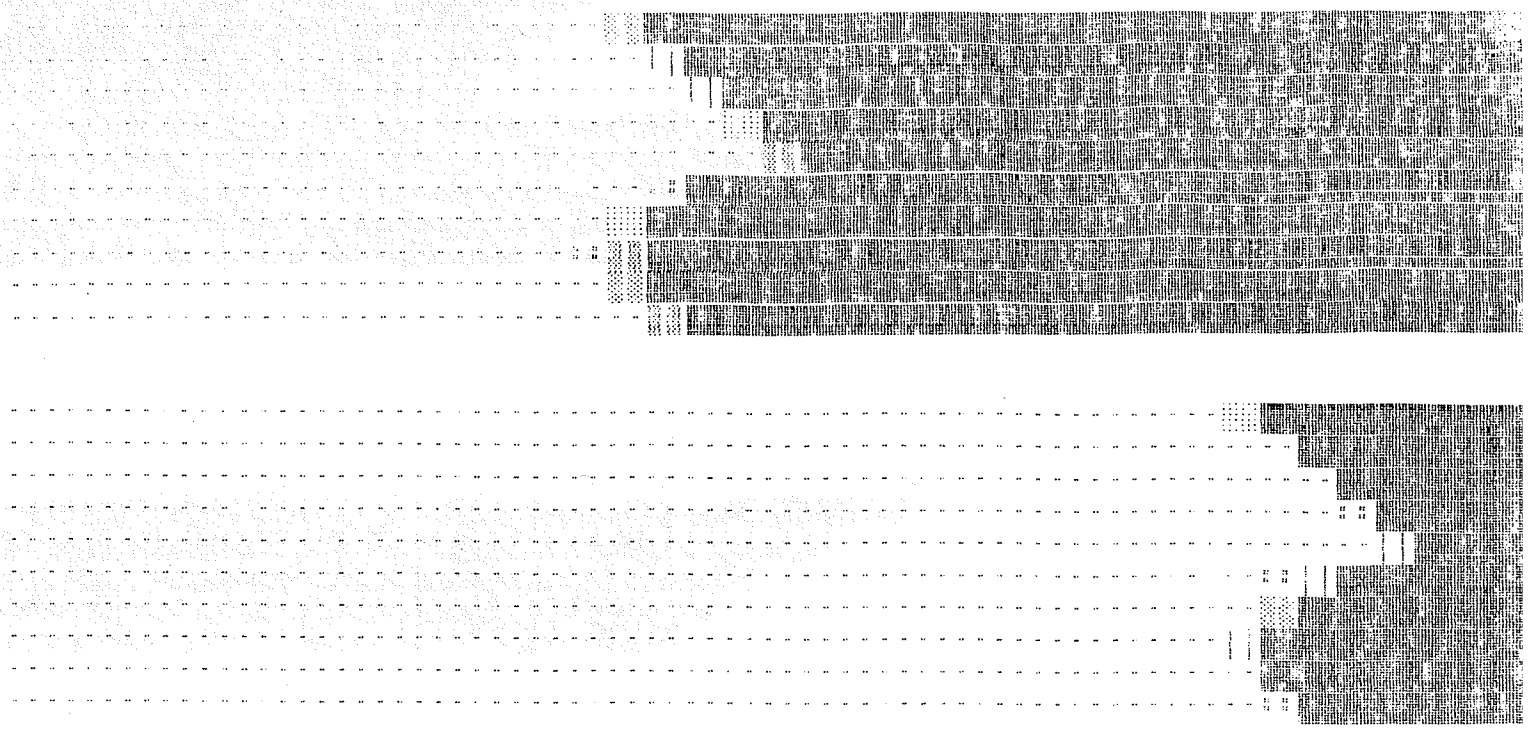

FIGURE 12. - ROS Distribution 2D (k_h = 462 md layer 1-5, k_h = 231 md layer 6-10, 40% shale between layer 5 and 6).

FIGURE 13. - ROS Distribution 2D (k_h = 462 md layer 1-5, k_h = 231 md layer 6-10, 100% shale between layers 5 and 6).

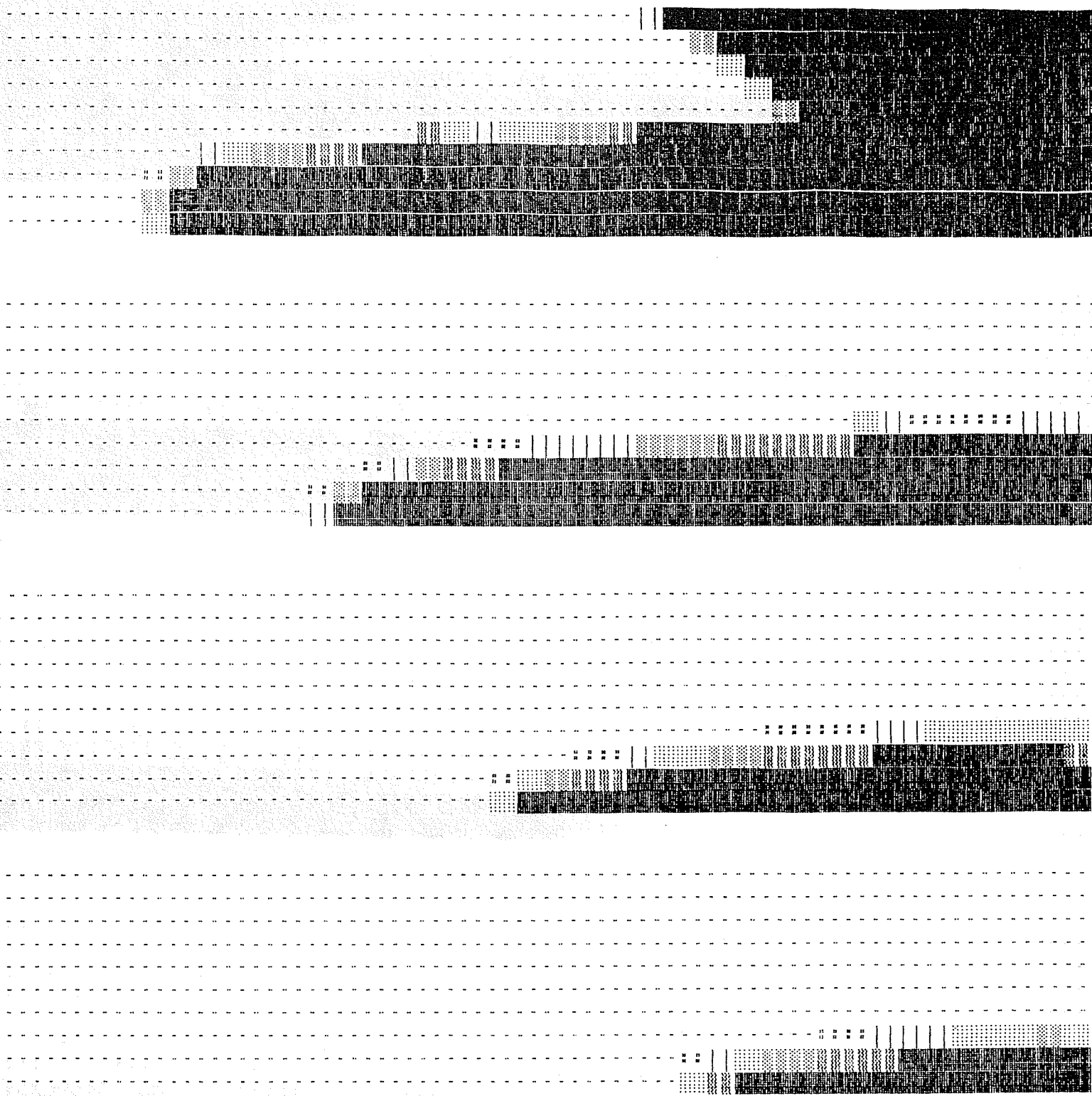

FIGURE 14. - ROS Distribution 2D (k_h = 630 md layer 1-5, k_h - 63 md layer 5-10, 10% shale between layers 5 and 6.

FIGURE 15. - ROS Distribution 2D (k_h = 630 md layer 1-5, k_h = 63 md layer 6-10, 40% shale between layers 5 and 6).

FIGURE 16. - ROS Distribution 2D, Case A (k_h = 346.5 md).

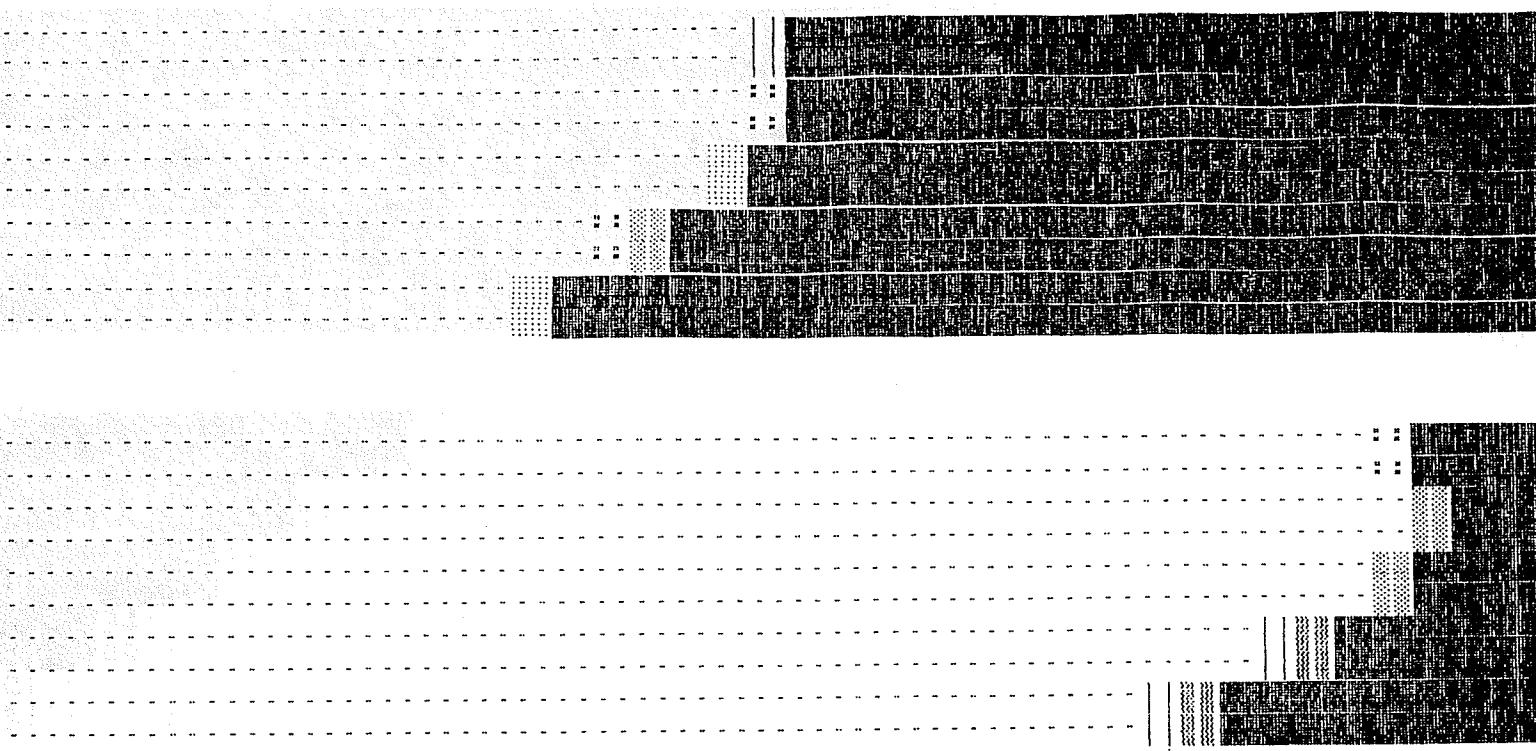

FIGURE 17. - ROS Distribution 2D, Case B ($k_{htop}/k_{hbottom}$ = 5, k_{htop} = 662.5 md).

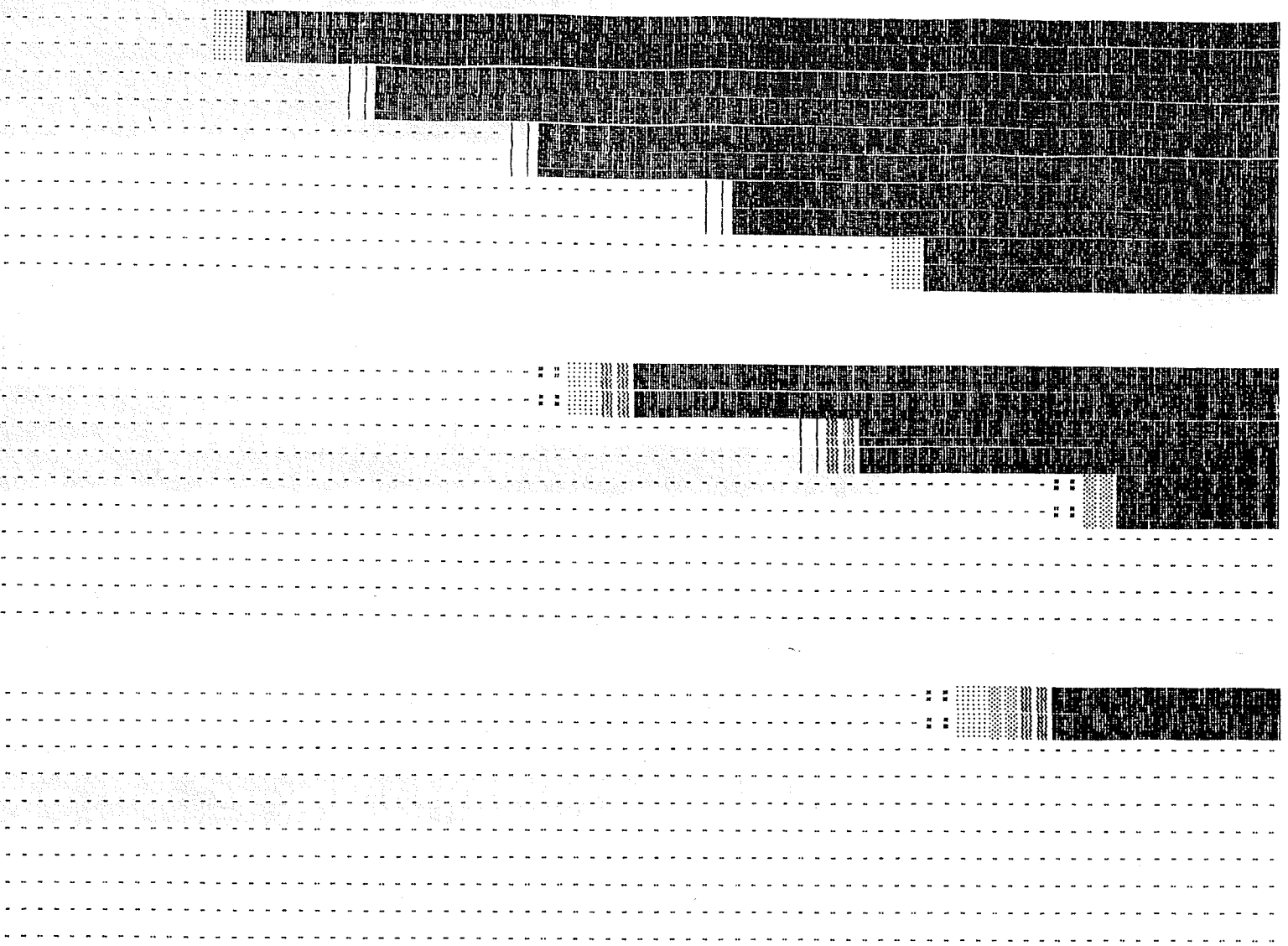

FIGURE 18. - ROS Distribution 2D, Case C ($k_{htop}/k_{hbottom}$ = 1/5, k_{htop} = 132.5 md).

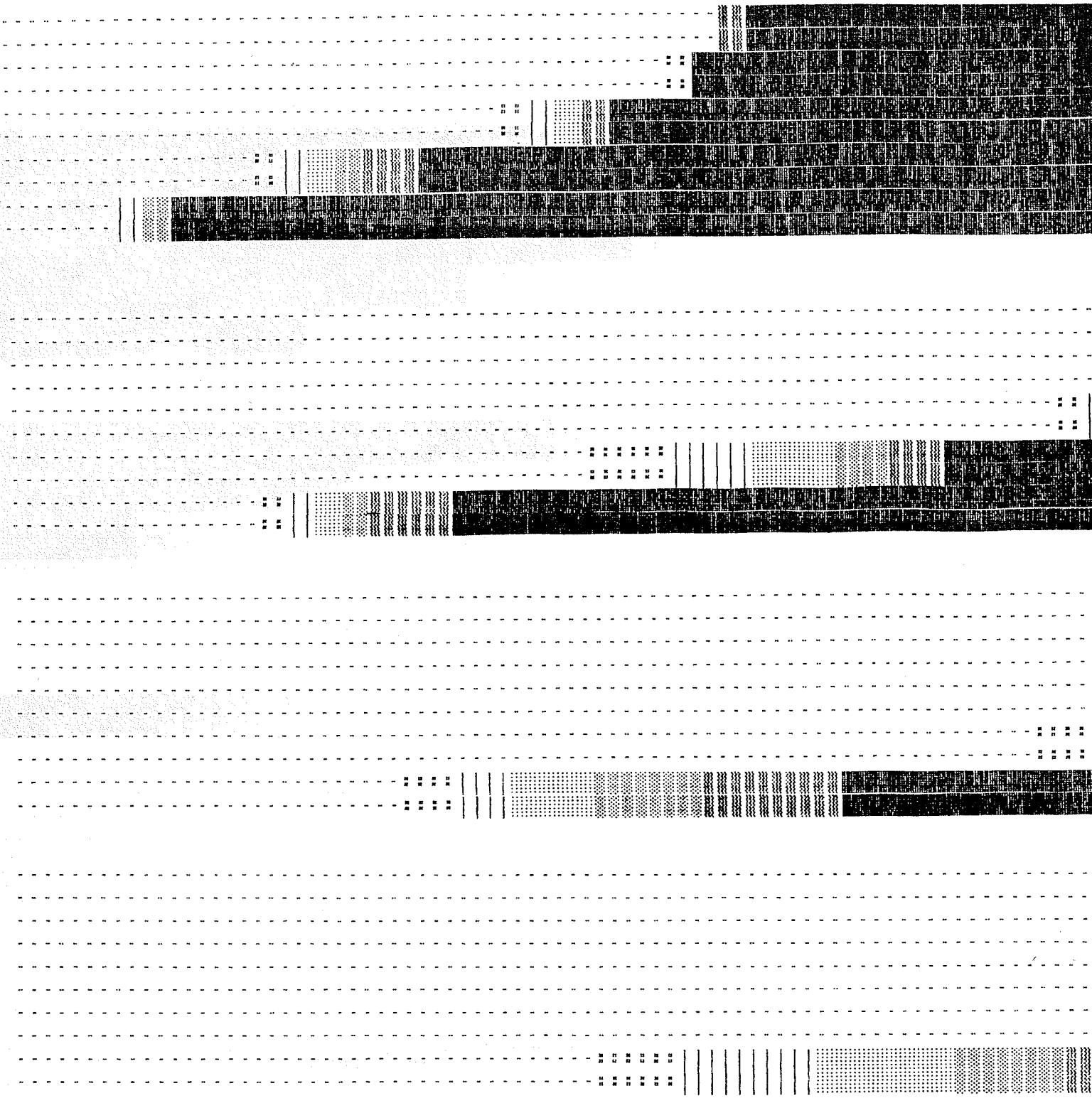

FIGURE 19. - ROS Distribution 2D, Case D ($k_{htop}/k_{hbottom}$ = 25, K_{htop} = 975.1 md).

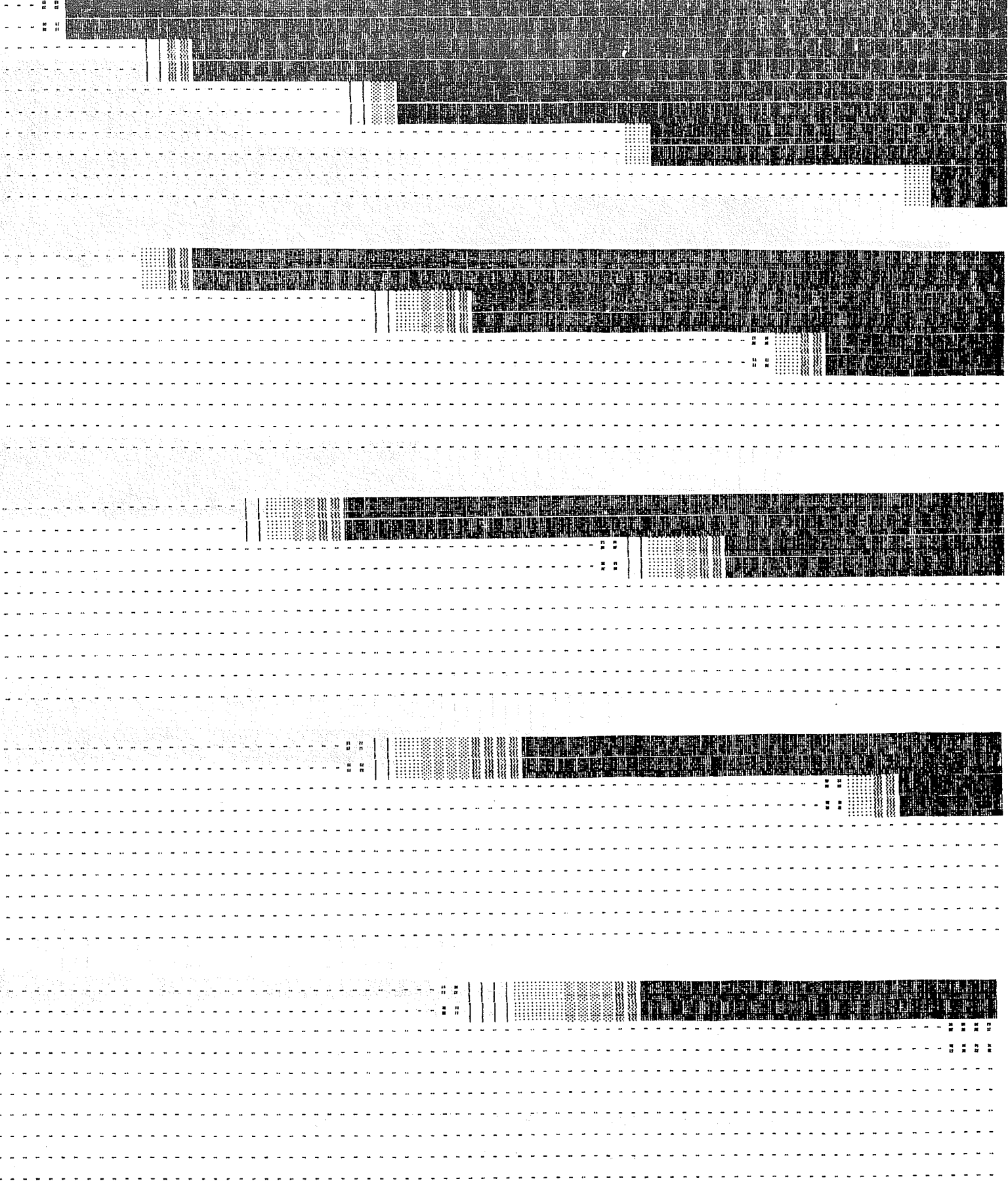

FIGURE 20. - ROS Distribution 2D, Case E ($k_{htop}/k_{hbottom}$ = 1/25, K_{htop} = 39 md).

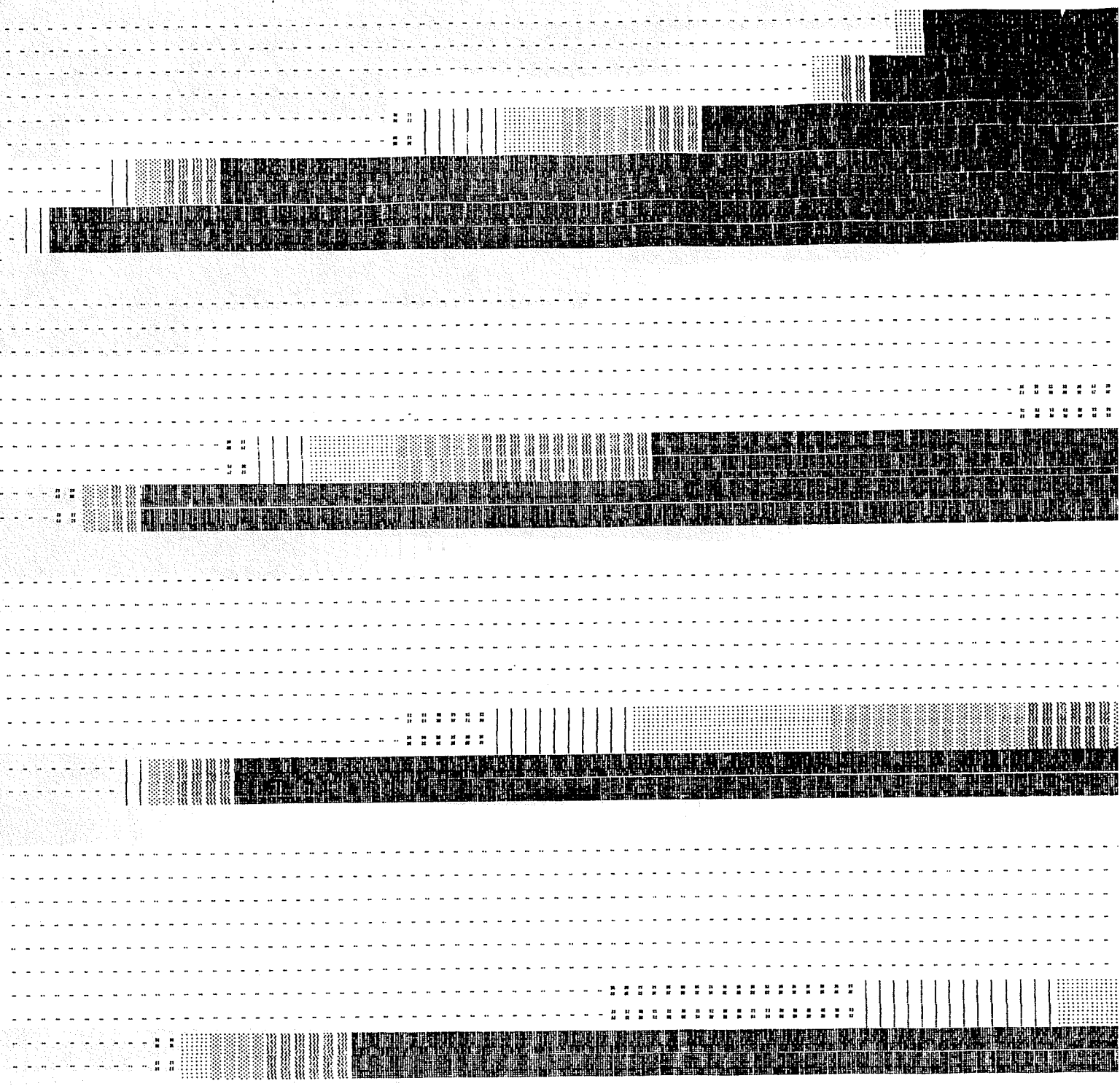

FIGURE 21. - ROS Distribution 2D, Case F (k_{htop}/k_{bottom} = 100, k_{htop} = 1189 md).

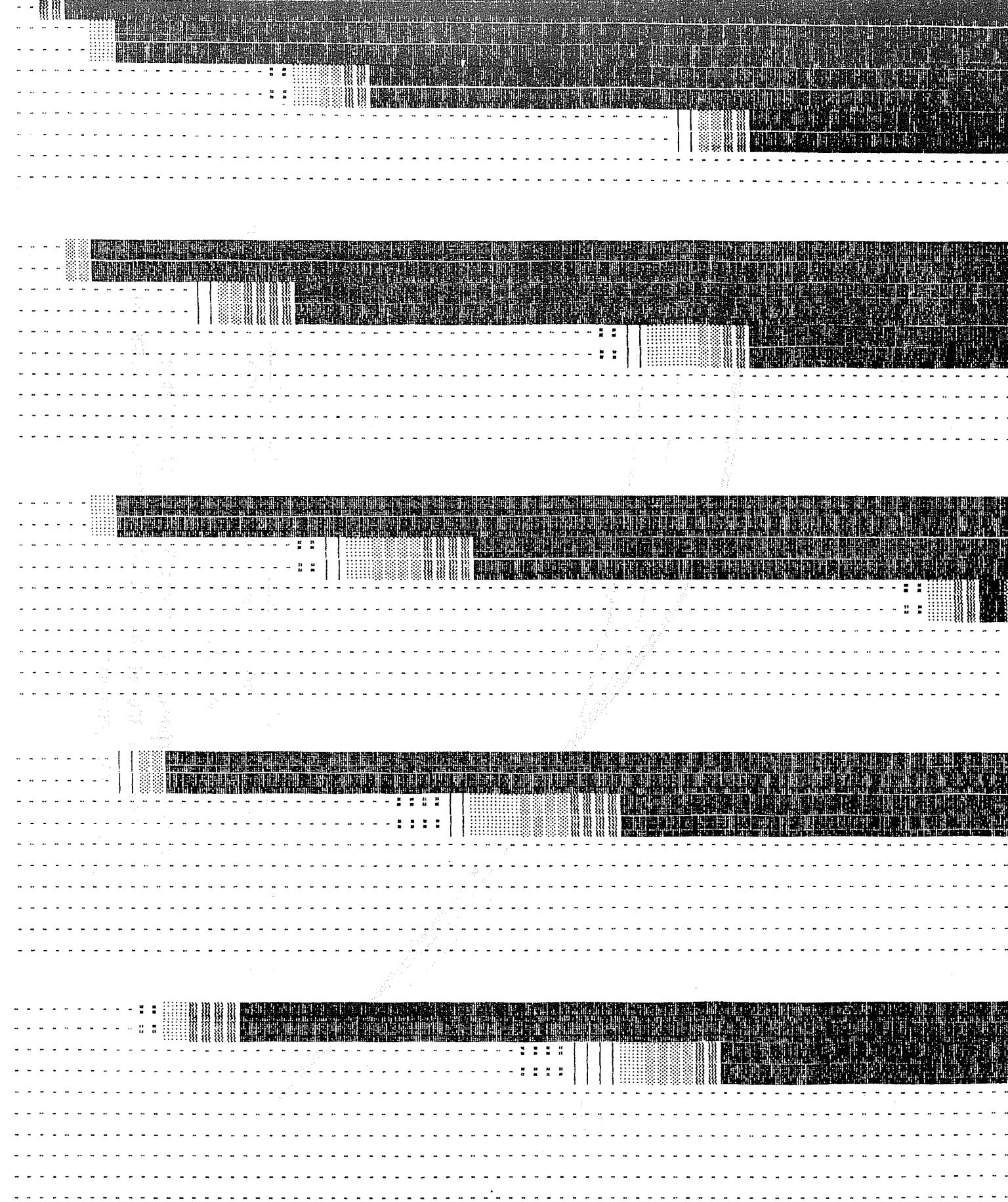

FIGURE 22. - ROS Distribution 2D, Case G ($k_{htop}/k_{hbottom}$ = 1/100, k_{htop} = 11.9 md).

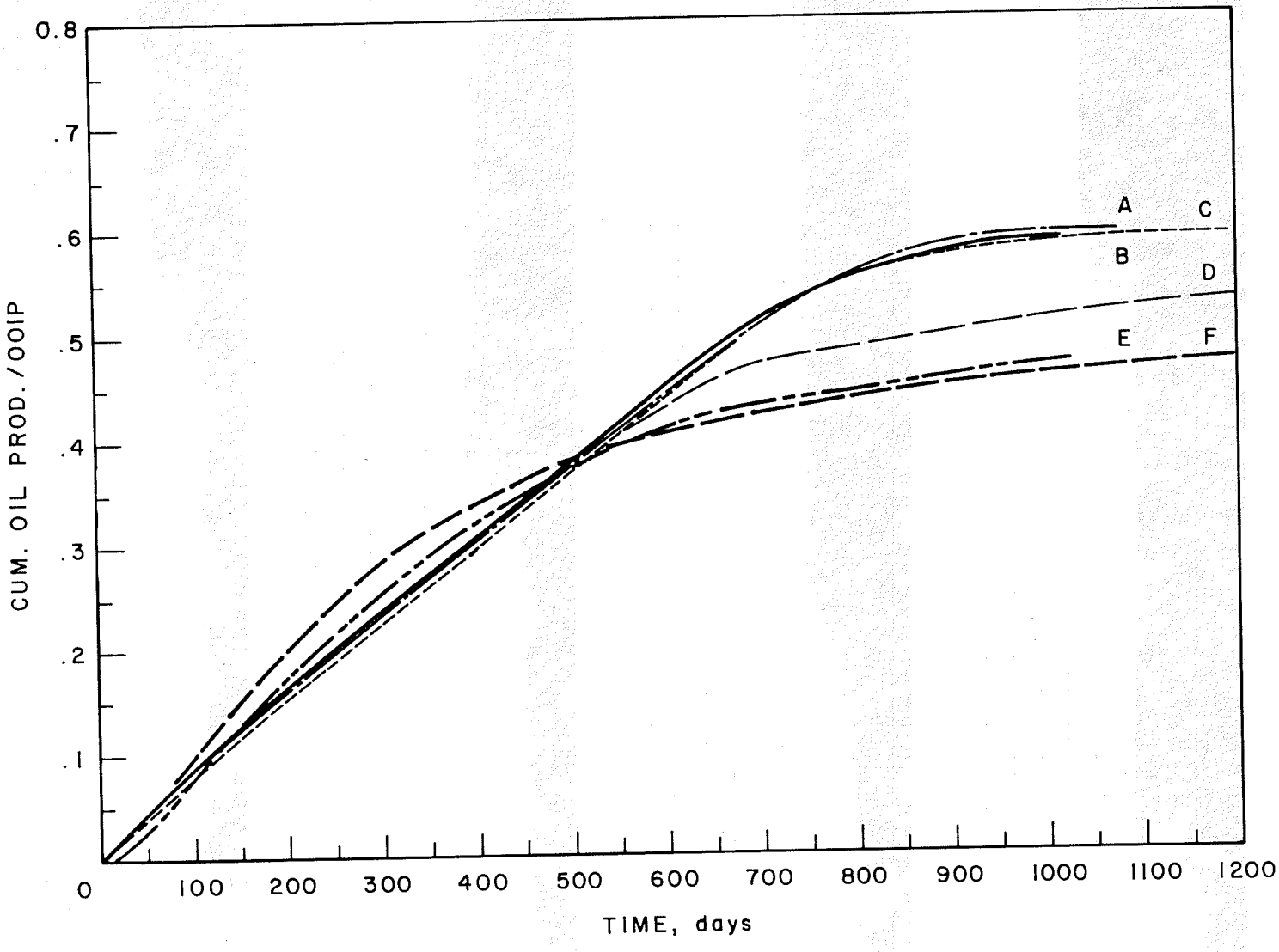

FIGURE 23. - Cumulative oil production (layers 5 and 6 of variable permeability: A) 300 md, B) 450 md, C) 600 md, D) 1,500 md, E) 3,000 md, F) 6,000 md).

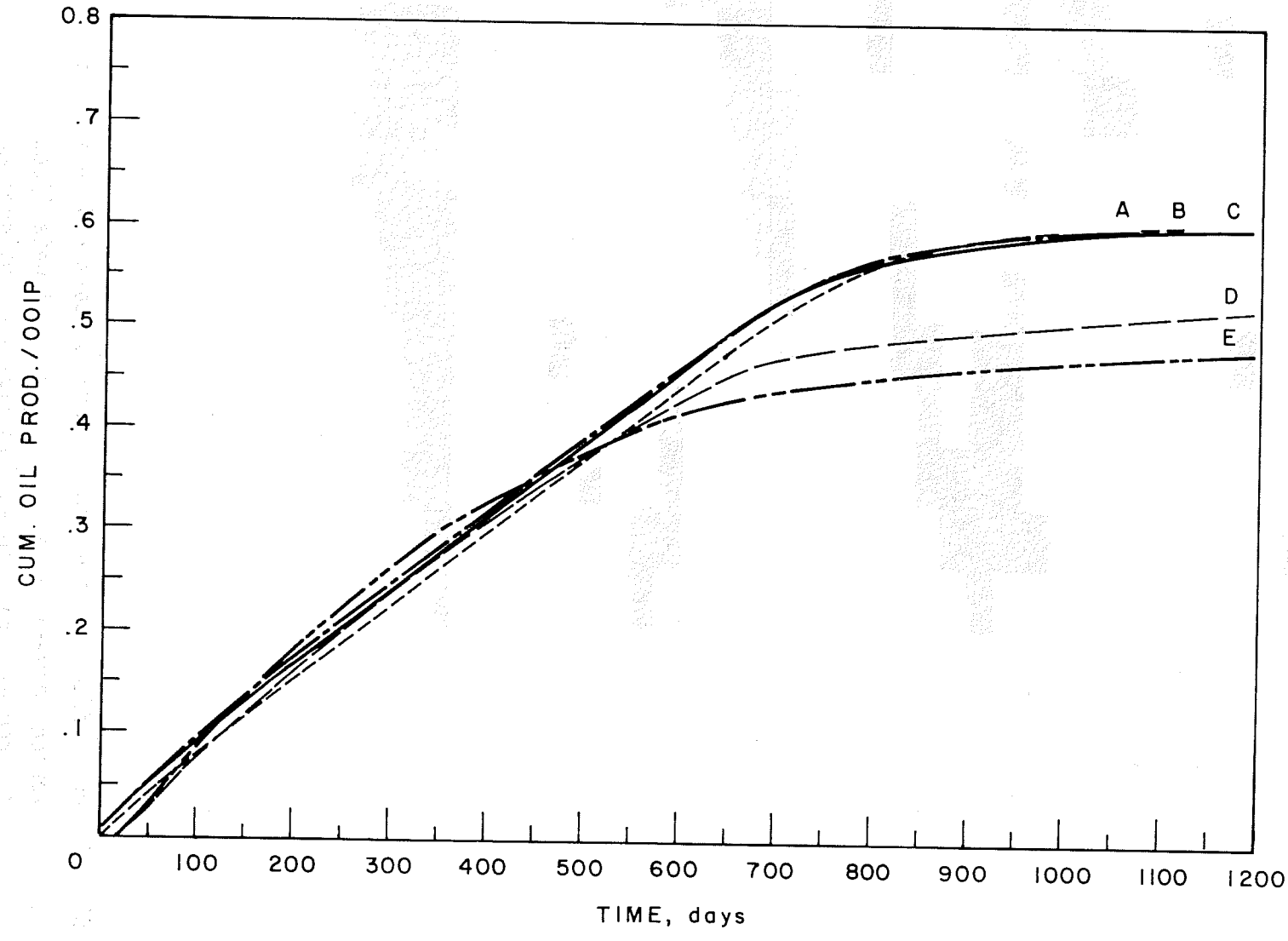

FIGURE 24. - Cumulative oil production, (layers 4, 5 and 6 of variable permeability, letter codes same as figure 23).

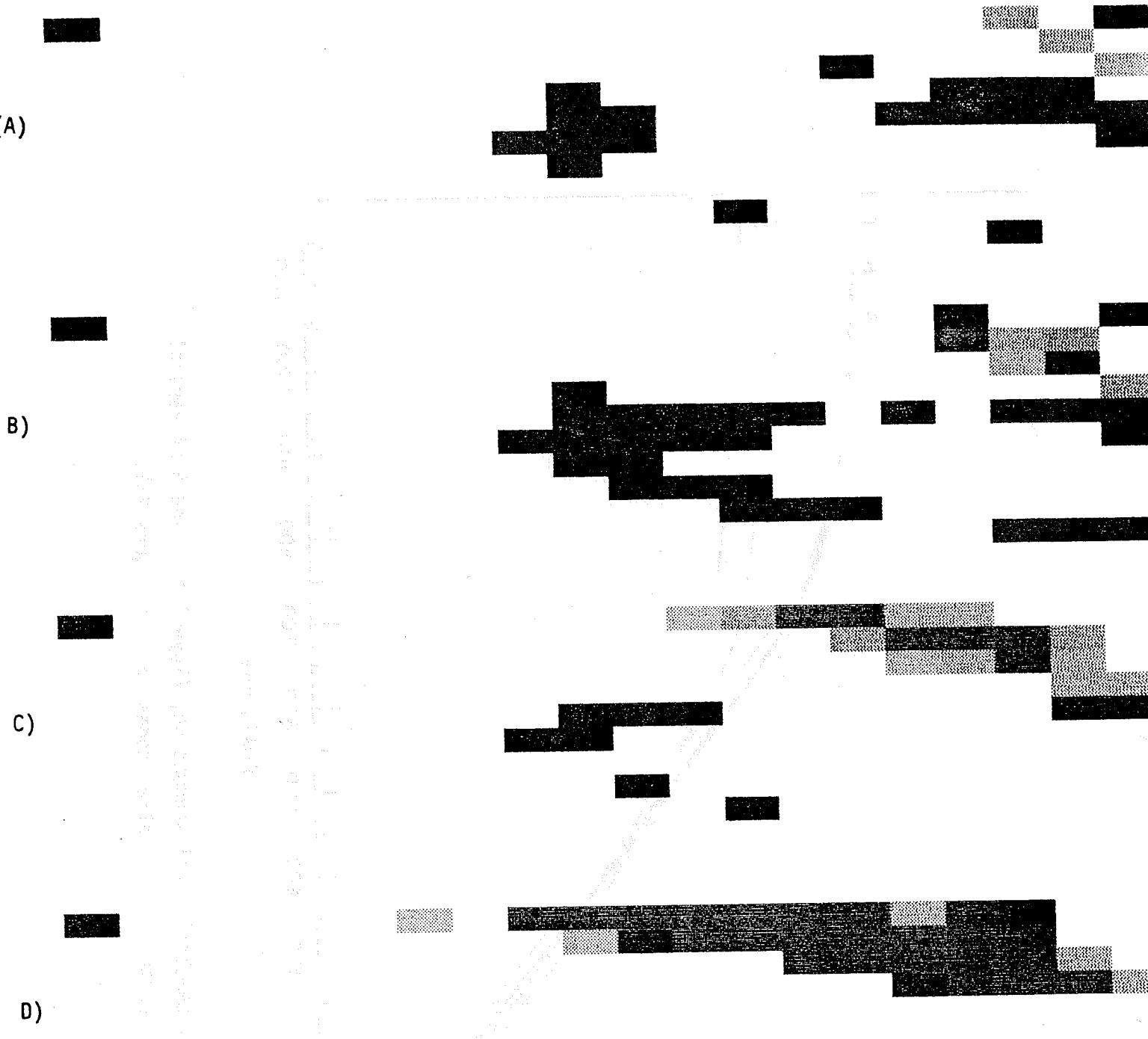

FIGURE 25. - ROS differences between homogeneous case and layer 5 of varied permeabilities after 2 years of waterflood: (A) 600 md, (B) 1500 md, (C) 3000 md, (D) 6000 md.

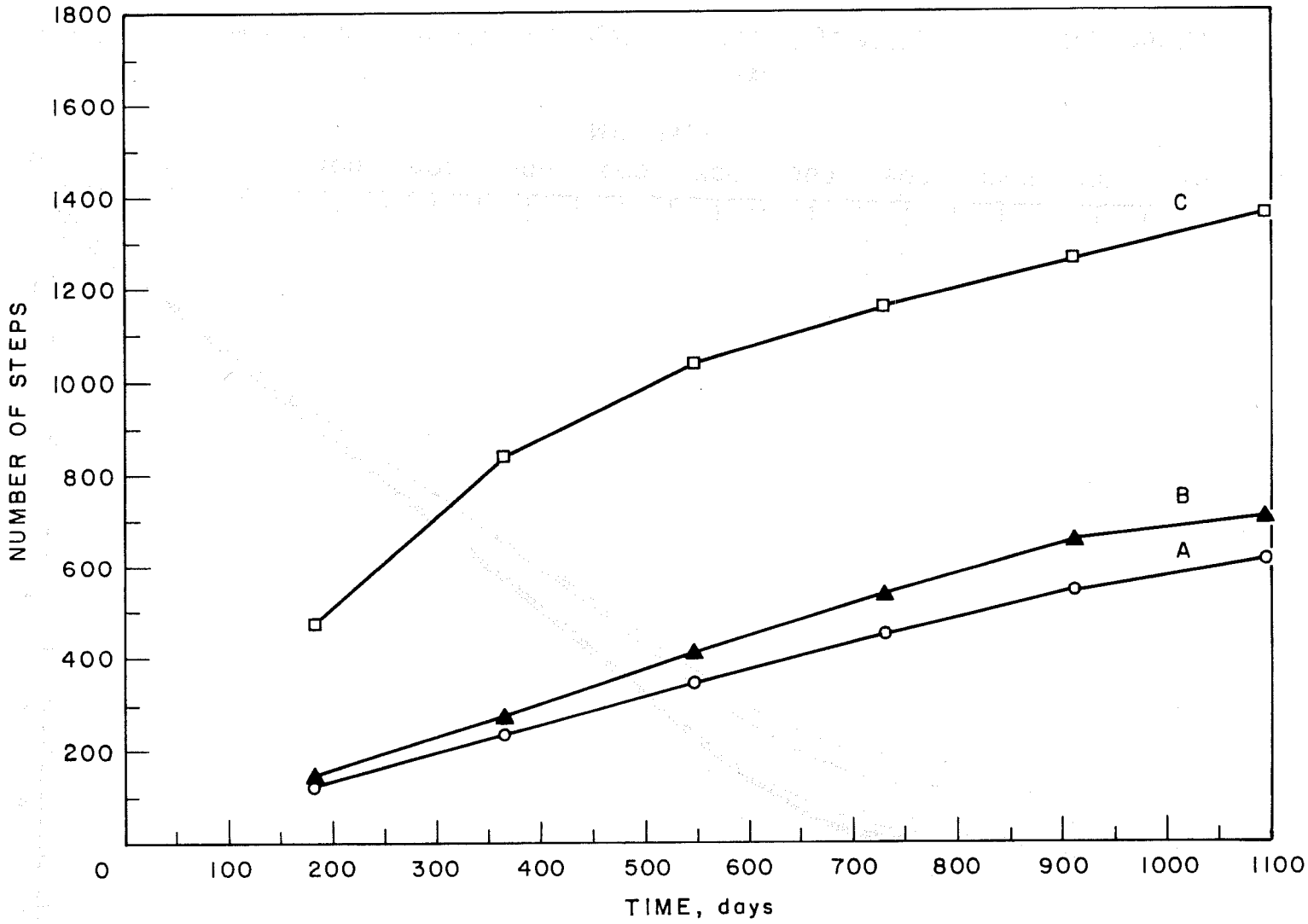

FIGURE 26. - Number of time stpes vs. waterflood time (layers 4, 5 and 6 of variable permeability: A) 300 md, B) 600 md, C) 6,000 md).

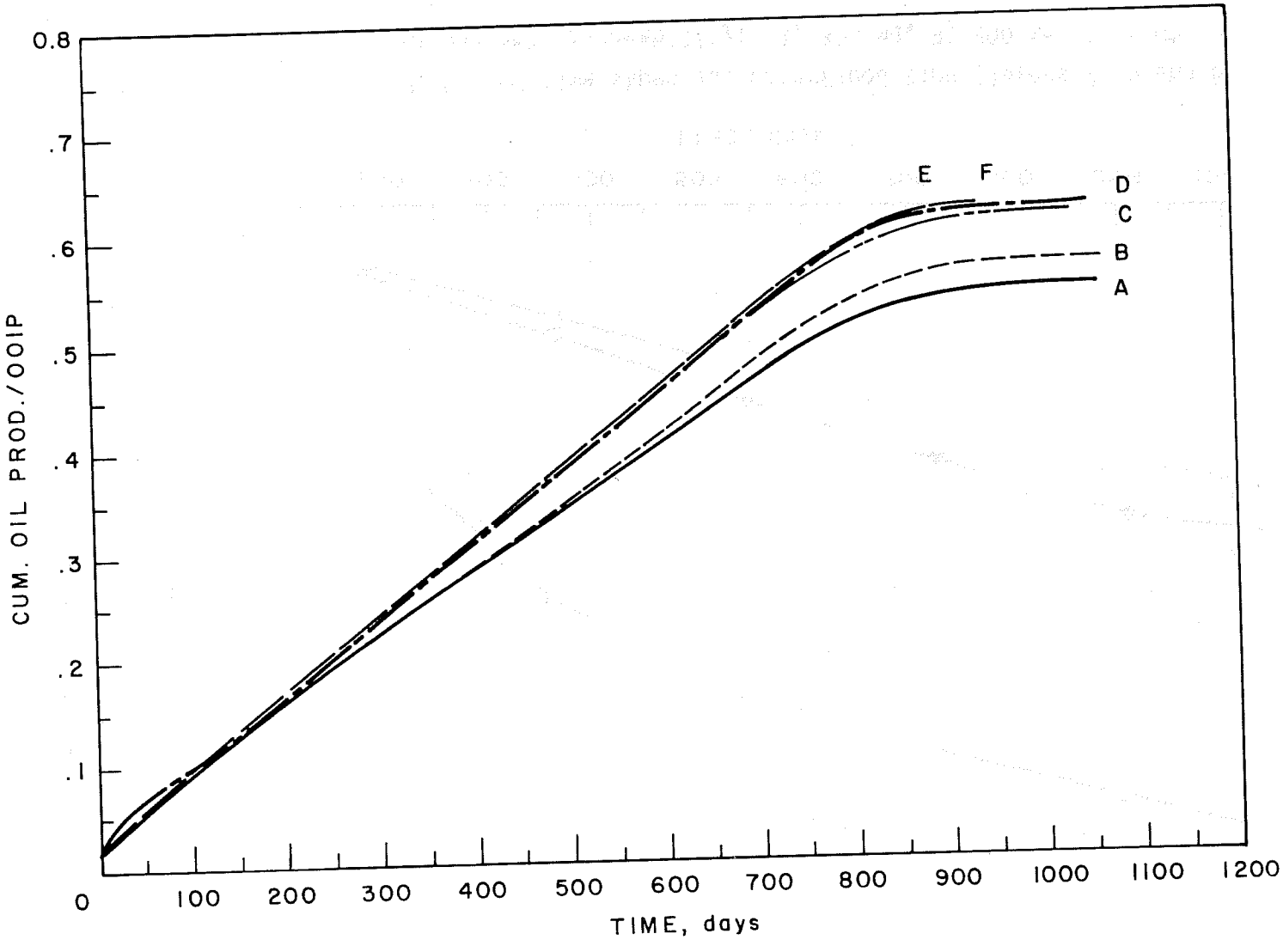

FIGURE. 27 - Cumulative oil production (k_h/k_z = 1(A), 2(B), 4(C), 10(D), 20(E), 40(F).

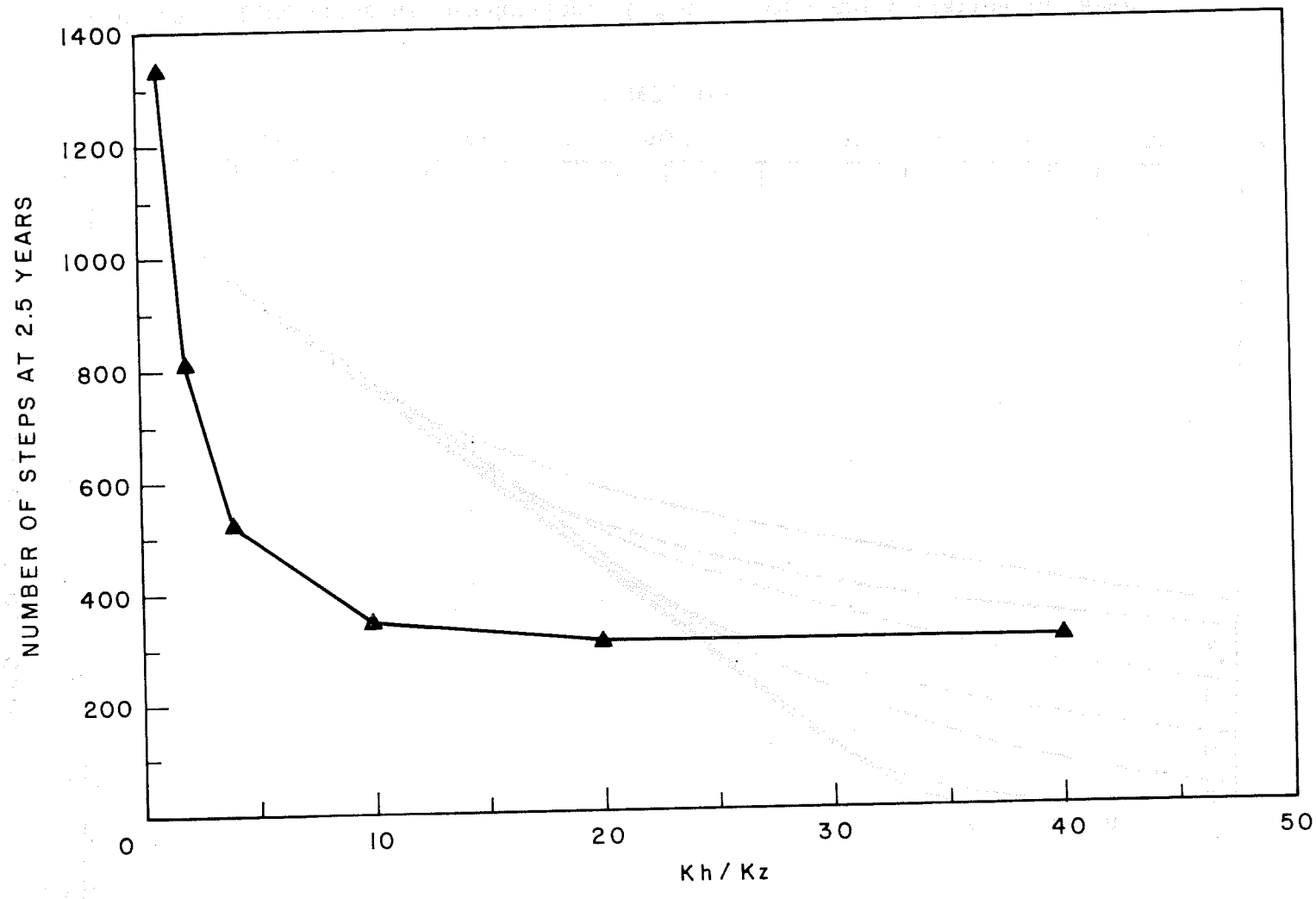

FIGURE 28. - Effect of vertical permeability on number of simulation time steps.

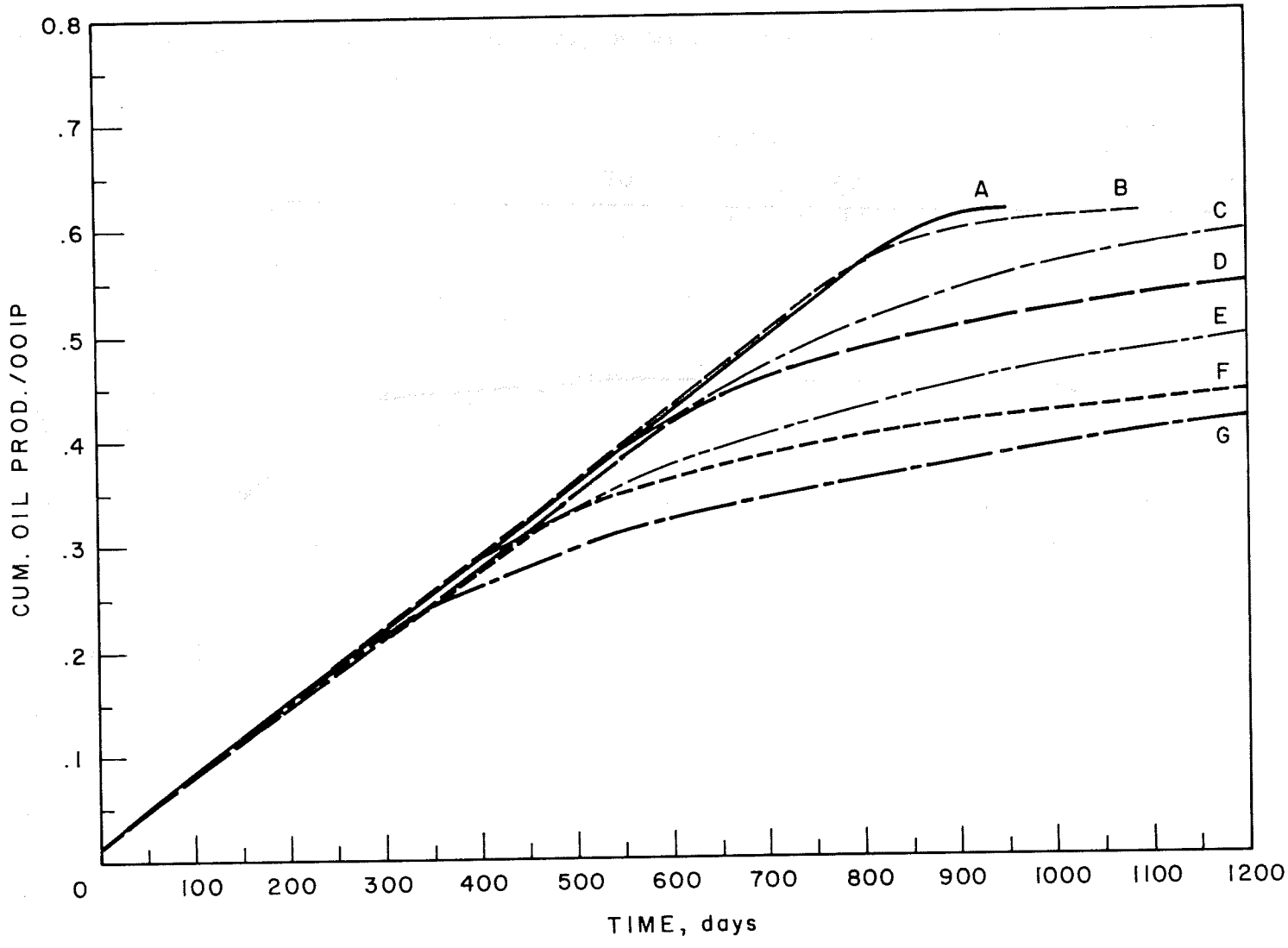

FIGURE 29. - Cumulative oil production. Effect of vertical variation in layers permeability (k_{top}/k_{bottom} = 1(A), 5(B), 1/5(C), 25(D), 1/25(E), 100(F), 1/100(G).

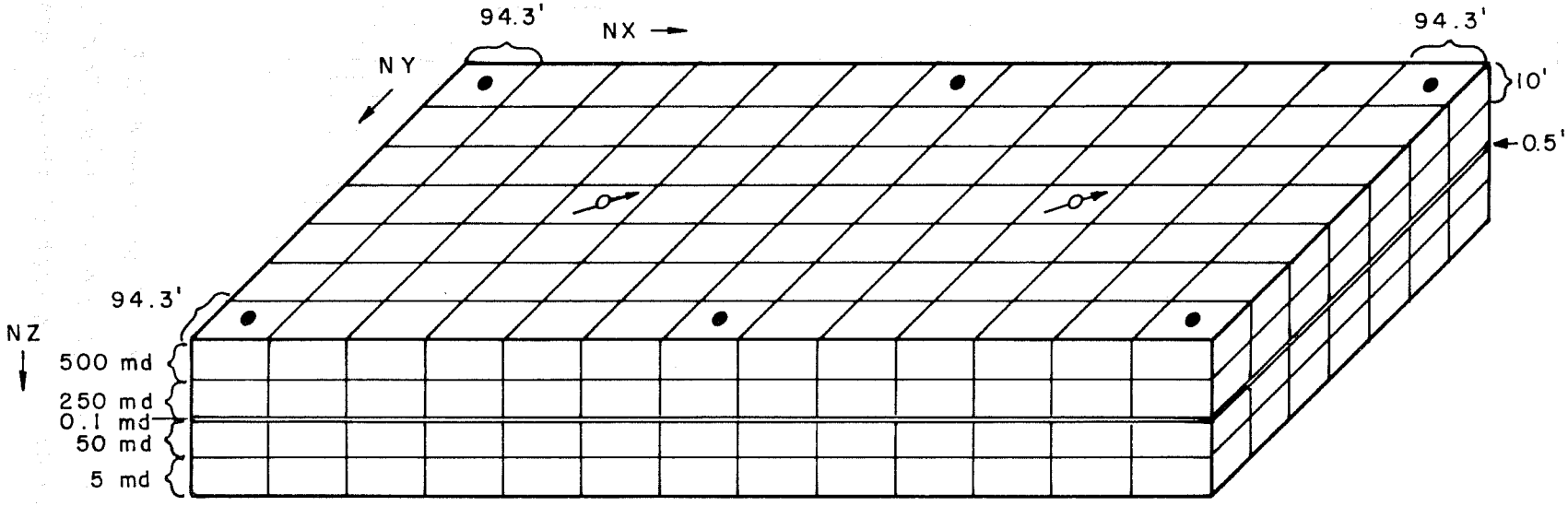

FIGURE 30. - Two inverted five-spot configuration.

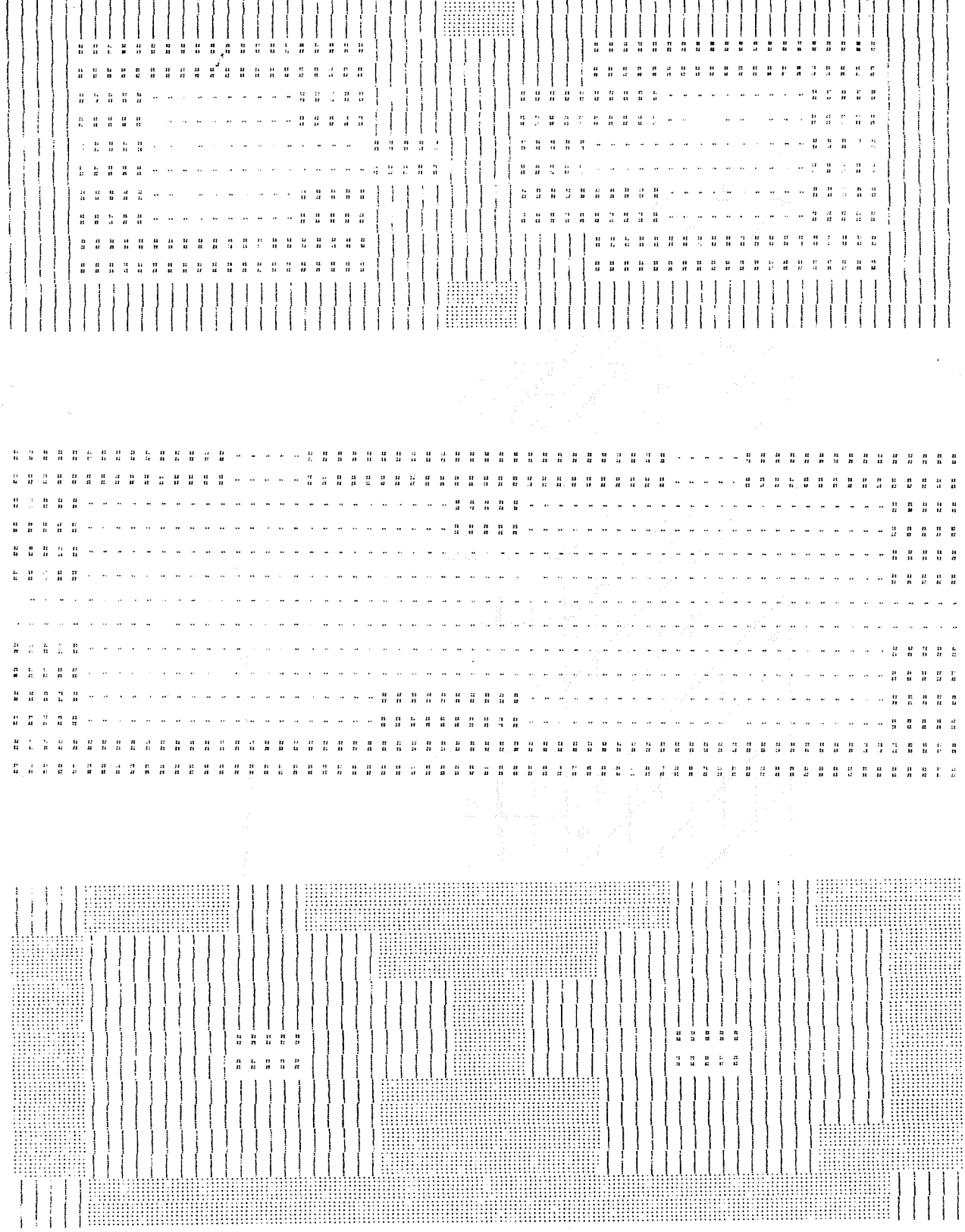

FIGURE 31. - ROS Distribution 3D case waterflood, year 4 (A-E: horizontal layers 1-5; F-H: vertical yz cross sections from most outward cross section (F) toward cross section through injector wells (H)).

D

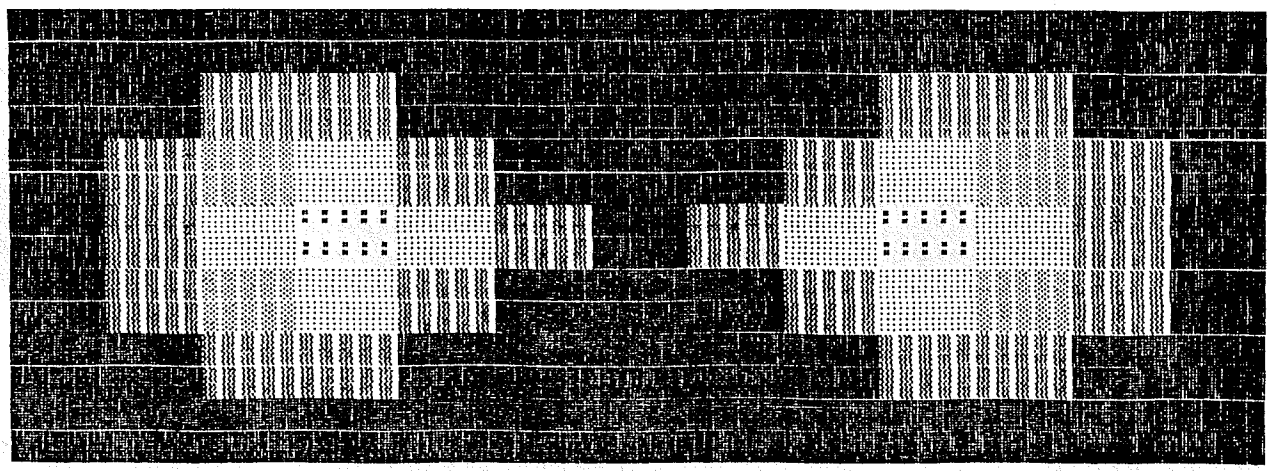

E

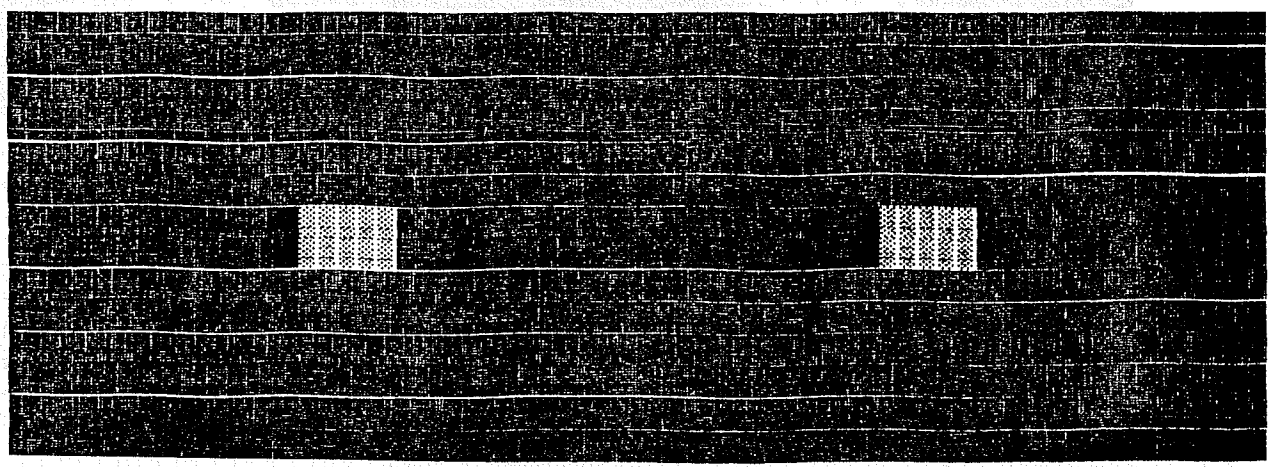

FIGURE 31. - (Continued)

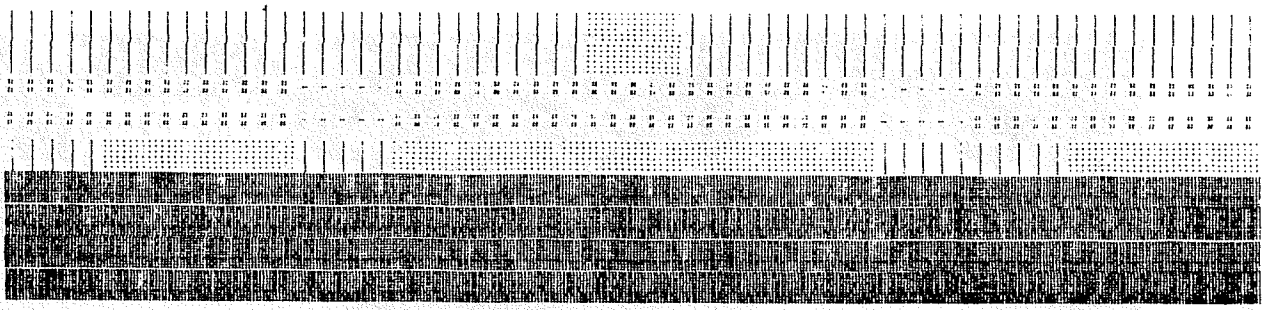

F

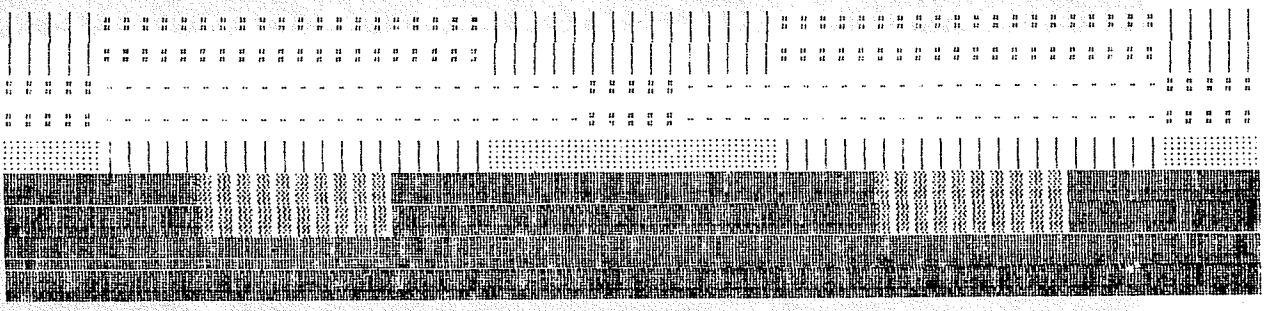

G

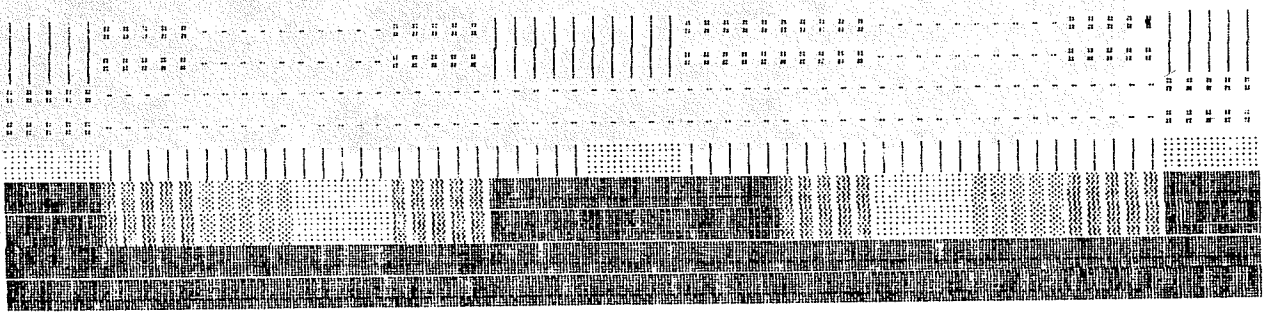

H

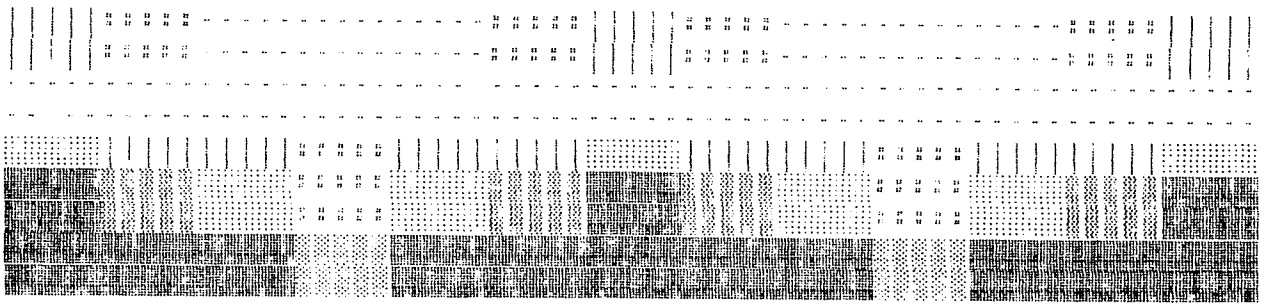

I

FIGURE 31. - (Continued)

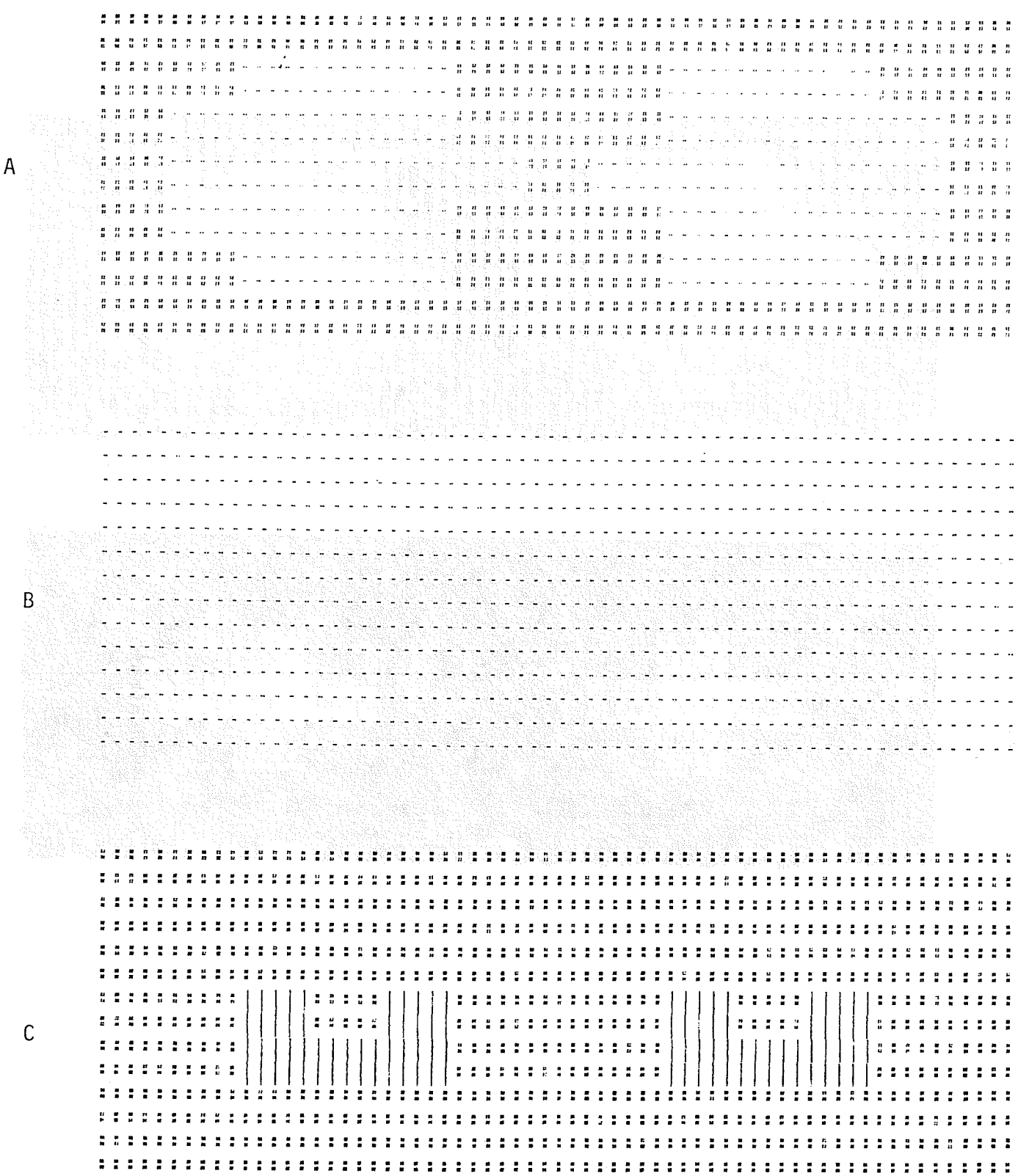

FIGURE 32. - ROS distributions 3D case; waterflood year 10 (same cross-sections as in figure 31).

D

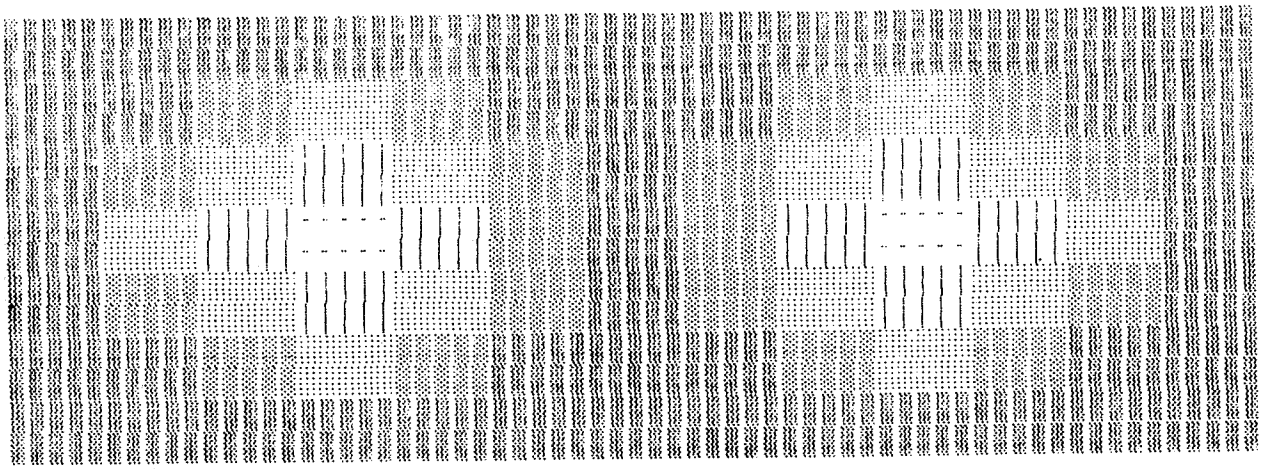

E

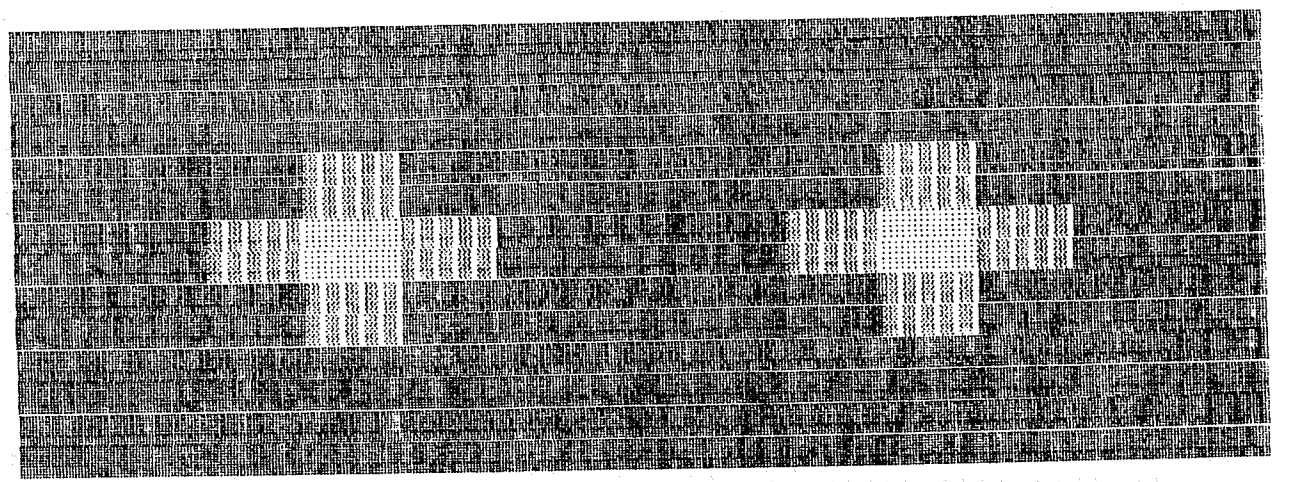

FIGURE 32. - (Continued)

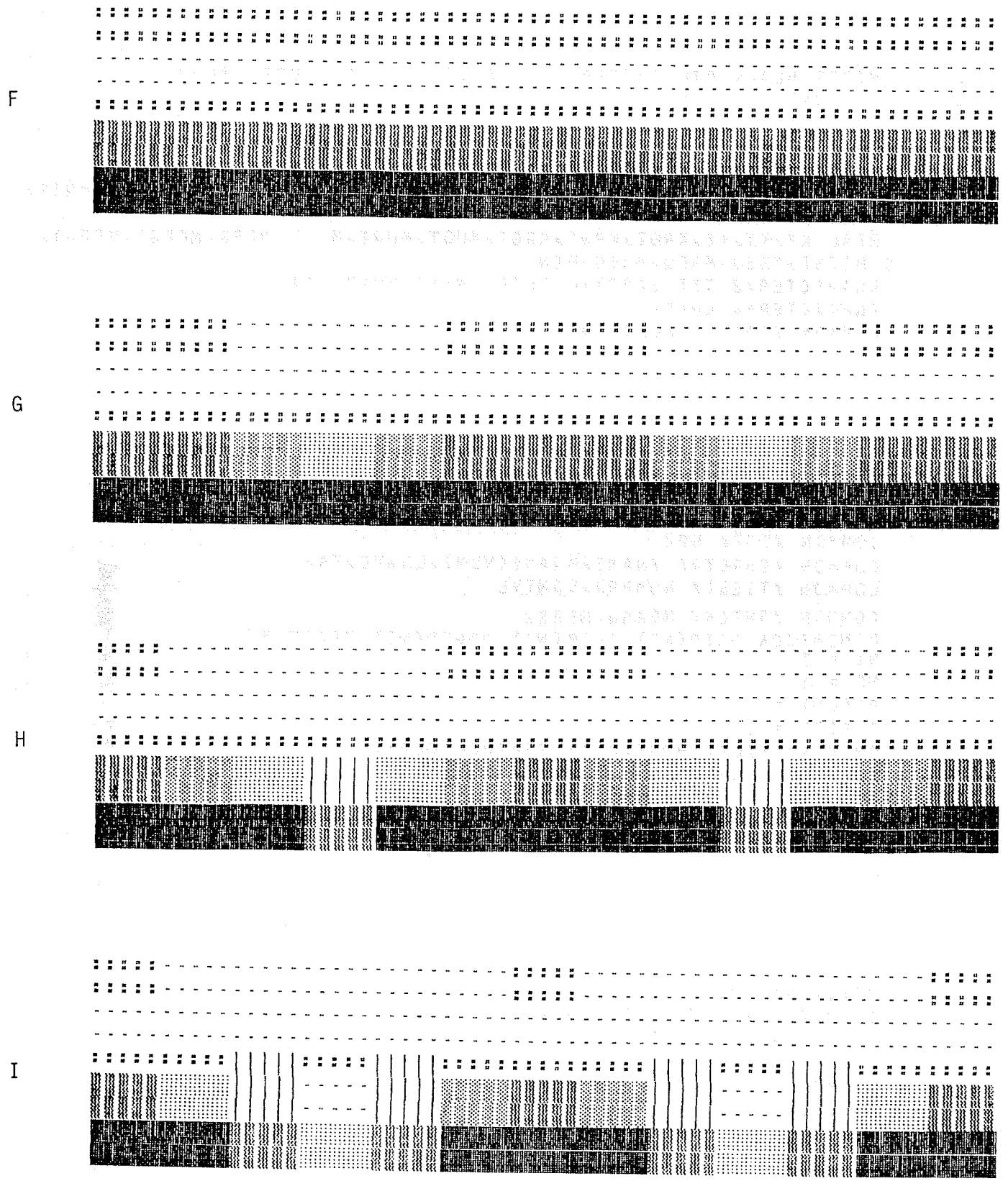

FIGURE 32. - (Continued)

```
C       NIPER BLACK OIL PRIMARY AND SECONDARY RECOVERY MODEL
C       FEBRUARY 8,1985
C
        PARAMETER(NX=80,NY=1,NZ=20,NTE=25,NW=2,NUM=40,
       & NXP=NX+1,NYP=NY+1,NZP=NZ+1,
       & MAX=NX*NY*NZ,NXPYZ=NXP*NY*NZ,NXYPZ=NX*NYP*NZ,NXYZP=NX*NY*NZP,
       & NWZ=NW*NZ)
        REAL KX,KY,KZ,KROT,KRWT,KRGT,MUOT,MUWT,MUGT,MCFG,MCFG1,MCFGT,
       & MCFGI,MBEO,MBEW,MBEG,MIN
        CHARACTER*2 TITLE(80),WELLID,FNAME,MNAME,TAG
        CHARACTER*4 LNAME
        COMMON /IDEN/ WELLID(NW)




        COMMON /PRTCNT/ IWLCNG,ICHANG,IWLREP,ISUMRY,
       & IPMAP,ISOMAP,ISWMAP,ISGMAP,IPBMAP
        COMMON /IO2/ NO2
        COMMON /CHRCTR/ FNAME,MNAME(NUM),LNAME,TAG
        COMMON /TTEST/ NUMPRD,SONTVL
        COMMON /SWTCH/ NGRSW,NTRSW
        DIMENSION OOIP(NZ),OWIP(NZ),ODGIP(NZ),OFGIP(NZ)
        NI = 5
        NO = 6
        DIFCNT = 0
        DIFTOT = 0
        OPEN(NI,FILE='BOST.DAT',STATUS='OLD')
        OPEN(NO,FILE='BOST.OUT',STATUS='NEW')
        OPEN(14,FILE='RATES.OUT',STATUS='NEW')
C        OPEN(24,FILE='PRESSURE.OUT',RECL = 201,STATUS='UNKNOWN')
        WRITE(NO,3005)




        SG(I,J,K)=0.0
        IF(SO(I,J,K).LT.0.5) THEN
         SW(I,J,K)=1.0-SO(I,J,K)
        ELSE
         TEMP = SO(I,J,K)
         SO(I,J,K)=1.0-SW(I,J,K)
        ENDIF
  405 CONTINUE
```

```
      IF(IWLREP.EQ.0) GO TO 2050
      IF(FT.GT.0.999.AND.FT.LT.1.001) GO TO 891
      IF(ABS(FT-NUMPRD*SONTVL).GT.0.001) GO TO 2050
  891 IF(IJ.EQ.1.AND.K.EQ.IQ3)WRITE(NO,591)FT




      IF(IWLREP.EQ.0)GO TO 2052
      IF(FT.GT.0.999.AND.FT.LT.1.001) GO TO 791
      IF(ABS(FT-NUMPRD*SONTVL).GT.0.001) GO TO 2052
  791 WRITE(NO,5912)TOR,TGR,TWR,TOC,TGC,TWC




C***** SUMMARY REPORT.
      WRITE(14,987) ETI,PAVG,OPR,GPR,WPR,WOR,GOR
C       WRITE(24,*) ETI
C       WRITE(24,986) ((P(I,1,K),I=1,40),K=1,10)
 987  FORMAT(7(F8.2,2X))
C 986  FORMAT(' ',40F5.0)
      IF(ISUMRY.EQ.0) GO TO 2057
      IF(NGRSW.EQ.1.AND.ABS(ETI-NUMPRD*SONTVL).LE.0.001) CALL GRPHCS
      NLP=N+1
      IF(FT.GT.0.999.AND.FT.LT.1.001) GO TO 691
      IF(ABS(ETI-(NUMPRD-1)*SONTVL).GT.0.001) GO TO 2057
  691 CALL PRTPS(NLP,DELTO)
```

```
C
      BLOCK DATA FILNAM
C
C=============================================BLOCK DATA FILNAM
C
C     CHARACTER VARIABLE INITIALIZATION FOR GRAPHICS.
C
C=================================================================
C
      PARAMETER(NUM=40)
      CHARACTER*2 FNAME,MNAME,TAG
      CHARACTER*4 LNAME
      COMMON /CHRCTR/ FNAME,MNAME(NUM),LNAME,TAG
      COMMON /TTEST/ NUMPRD,SONTVL
      COMMON /IO2/ NO2
      DATA NO2/7/
      DATA NUMPRD/1/
      DATA FNAME,LNAME/'SO','.DAT'/
      DATA MNAME/'01','02','03','04','05','06','07','08','09',
     & '10','11','12','13','14','15','16','17','18','19','20',
     & '21','22','23','24','25','26','27','28','29','30','31',
     & '32','33','34','35','36','37','38','39','40'/
      END
```

SUBROUTINE GRID1

```
      COMMON /VECTOR/ DX(NX,NY,NZ),DY(NX,NY,NZ),DZ(NX,NY,NZ)
      COMMON /SWTCH/ NGRSW,NTRSW
      DIMENSION SUM(NX,NY),VAREL(NX,NY),PDXL(NX),RDYL(NY),RDZL(NZ)
      READ(NI,69) (TITLE(IH),IH=1,40)
      WRITE(NO,70) (TITLE(IH),IH=1,40)
      READ(NI,*) II,JJ,KK
      READ(NI,69) (TITLE(IH),IH=1,40)
      READ(NI,*) NGRSW,NTRSW
      IF(NGRSW.EQ.1) CALL GRINT
      READ(NI,69) (TITLE(IH),IH=1,40)
```

SUBROUTINE TRAN1

```
      COMMON /CODE/ KSM1,KSN1,KCO1,NN,FACT1,FACT2,TMAX,KSOL,MITER,
     & OMEGA,TOL,TOL1,KSN,KSM,KCO,KTR,KCOFF,DSMAX,DPMAX,WORMAX,
     & GORMAX,PAMIN,PAMAX
      COMMON /SWTCH/ NGRSW,NTRSW
C
      REAL KX,KY,KZ


C****** TRANSMISSIBILITY MODIFICATIONS
C
      IF(NTRSW.EQ.1) CALL SHALE
      READ(NI,69) (TITLE(IH),IH=1,40)
```

```
C
C
      SUBROUTINE GRINT
C
C=============================================================GRINT
C
C    READS DATA FOR GRAPHICS INITIALIZATION PURPOSES.
C
C=============================================================
C
      PARAMETER(NUM=40)
      CHARACTER*2 TITLE(80),FNAME,MNAME,TAG
      CHARACTER*4 LNAME
      COMMON /CHRCTR/ FNAME,MNAME(NUM),LNAME,TAG
      COMMON /TTEST/ NUMPRD,SONTVL
      COMMON /IO/ NI,NO
      READ(NI,69) (TITLE(IH),IH=1,40)
   69 FORMAT(40A2)
      READ(NI,70) TAG
   70 FORMAT(A2)
      READ(NI,*) SONTVL
      RETURN
      END
C
C
C
      SUBROUTINE GRPHCS
C
C=============================================================GRPHCS
C
C    WRITES THE OIL SATURATION FILES.
C
C=============================================================
C
      PARAMETER(NX=80,NY=1,NZ=20,NUM=40)
      CHARACTER*2 FNAME,MNAME,TAG
      CHARACTER*4 LNAME
      CHARACTER*10 TNAME
      COMMON /CHRCTR/ FNAME,MNAME(NUM),LNAME,TAG
      COMMON /TTEST/ NUMPRD,SONTVL
      COMMON /IO2/ NO2
      COMMON /NUMBER/ II,JJ,KK
      COMMON /PRTS/ SO(NX,NY,NZ),SW(NX,NY,NZ),SG(NX,NY,NZ)
      TNAME=TAG//(FNAME//(MNAME(NUMPRD)//LNAME))
      OPEN(NO2,FILE=TNAME,STATUS='UNKNOWN')
      DO 10 K=1,KK
      DO 10 J=1,JJ
      WRITE(NO2,20) (SO(I,J,K),I=1,II)
   20 FORMAT(10F7.3)
   10 CONTINUE
      CLOSE(NO2,STATUS='KEEP')
      NUMPRD=NUMPRD+1
      RETURN
      END
C
```

```
C
      SUBROUTINE SHALE
C
C=============================================================SHALE
C
C     ALLOWS BROAD ZEROING OF TRANSMISSIBILITIES FOR THE
C     PURPOSE OF SIMULATING SHALES.
C
C=============================================================
C
      PARAMETER(NX=80,NY=1,NZ=20)
      CHARACTER*2 TITLE(80)
      COMMON /IO/ NI,NO
      COMMON /TRAN/ TX(NX+1,NY,NZ),TY(NX,NY+1,NZ),TZ(NX,NY,NZ+1)
      COMMON /NUMBER/ II,JJ,KK
      READ(NI,69) (TITLE(IH),IH=1,40)
   69 FORMAT(40A2)
      READ(NI,*) NSHOPS
      READ(NI,*) NTLAYR
      IF(NSHOPS.EQ.1) THEN
      DO 1 LZ=1,NTLAYR
      READ(NI,*) KT
      DO 1 JLZ=1,JJ
      DO 1 ILZ=1,II
      TZ(ILZ,JLZ,KT)=0.0
    1 CONTINUE
      ELSE
      DO 2 LZ=1,NTLAYR
      READ(NI,*) KT,NUTM
      DO 2 LZF=1,NUTM
      READ(NI,*) IGBL
      DO 2 JLZ=1,JJ
      TZ(IGBL,JLZ,KT)=0.0
    2 CONTINUE
      ENDIF
      RETURN
      END
```

```
180 REM*************************************************************************
190 REM*                              MAIN                                     *
200 REM*                                                                       *
210 REM*   The main program displays menus, prompts input, initializes         *
220 REM*      color and character plot arrays, and scales the output           *
230 REM*      screens.                                                         *
240 REM*                                                                       *
250 REM*************************************************************************
260 INPUT "NUMBER OF GRID BLOCKS IN THE X-DIRECTION";X
270 INPUT "NUMBER OF GRID BLOCKS IN THE Y-DIRECTION";Y
280 INPUT "NUMBER OF GRID BLOCKS IN THE Z-DIRECTION";Z
290 DIM SO(X,Y,Z),XDIM(X),YDIM(Y),ZDIM(Z),XC(X),YC(Y),YR(Y),ZR(Z)
300 DIM COLRX(7),CHARX(7)
310 IF X=>Y THEN LARG=X: GOTO 330
320 LARG=Y
330 DIM LGTH(LARG+1),WDTH(LARG+1)
340 COLRX(1)=7:  CHARX(1)=255
350 COLRX(2)=4:  CHARX(2)=58
360 COLRX(3)=14: CHARX(3)=179
370 COLRX(4)=2:  CHARX(4)=176
380 COLRX(5)=1:  CHARX(5)=177
390 COLRX(6)=5:  CHARX(6)=178
400 COLRX(7)=0:  CHARX(7)=219
410 CLS
420 PRINT: PRINT "X-DIRECTION GRID DIMENSION INPUT OPTIONS": PRINT
430 PRINT 0,"ALL X-DIRECTION GRID DIMENSIONS EQUAL-AUTOMATIC INPUT"
440 PRINT 1,"X-DIRECTION GRID DIMENSIONS NOT EQUAL-MANUAL INPUT"
450 PRINT: INPUT "CHOICE";CHOICE
460 IF CHOICE>1 THEN GOTO 410
470 XSUM=0
480 FOR I=1 TO X
490 IF CHOICE=0 THEN XDIM(I)=1: GOTO 520
500 CLS
510 PRINT "COLUMN  ";I: INPUT "WIDTH OF COLUMN=";XDIM(I)
520 XSUM=XSUM+XDIM(I)
530 NEXT I
540 XSCALE=80/XSUM
550 CLS
560 PRINT: PRINT "Y-DIRECTION GRID DIMENSION INPUT OPTIONS": PRINT
570 PRINT 0,"ALL Y-DIRECTION GRID DIMENSIONS EQUAL-AUTOMATIC INPUT"
580 PRINT 1,"Y-DIRECTION GRID DIMENSIONS NOT EQUAL-MANUAL INPUT"
590 PRINT: INPUT "CHOICE";CHOICE
600 IF CHOICE>1 THEN GOTO 550
610 YSUM=0
620 FOR J=1 TO Y
630 IF CHOICE=0 THEN YDIM(J)=1: GOTO 660
640 CLS
650 PRINT "ROW  ";J: INPUT "LENGTH OF ROW=";YDIM(J)
660 YSUM=YSUM+YDIM(J)
670 NEXT J
680 YRSCAL=20/YSUM
690 YCSCAL=80/YSUM
700 CLS
710 PRINT: PRINT "LAYER THICKNESS (Z-DIMENSION) INPUT OPTIONS": PRINT
720 PRINT 0,"ALL Z-DIRECTION GRID DIMENSIONS EQUAL-AUTOMATIC INPUT"
730 PRINT 1,"Z-DIRECTION GRID DIMENSIONS NOT EQUAL-MANUAL INPUT"
740 PRINT: INPUT "CHOICE";CHOICE
750 IF CHOICE>1 THEN GOTO 700
760 ZSUM=0
770 FOR K=1 TO Z
780 IF CHOICE=0 THEN ZDIM(K)=1: GOTO 810
```

```
790  CLS
800  PRINT "LAYER  ";K: INPUT "THICKNESS OF LAYER=";ZDIM(K)
810  ZSUM=ZSUM+ZDIM(K)
820  NEXT K
830  ZSCALE=20/ZSUM
840  GOSUB 1300
850  CLS
860  MULT=X*Y
870  TEST=X*Y*Z
880  COUNT=0
890  INPUT "FILENAME";A$
900  OPEN A$ FOR INPUT AS #1
910  K=1
920  J=1
930  I=1
940  INPUT #1,SO(I,J,K)
950  IF SO(I,J,K)=0 THEN GOTO 940
960  COUNT=COUNT+1
970  IF COUNT=TEST THEN CLOSE: GOTO 1020
980  IF COUNT=K*MULT THEN K=K+1: GOTO 920
990  I=I+1
1000 IF I>X THEN J=J+1: GOTO 930
1010 GOTO 940
1020 CLS
1030 PRINT: PRINT "OPTIONS": PRINT
1040 PRINT 1,"X-Y PLANE        (COLOR GRAPHICS)"
1050 PRINT 2,"X-Z PLANE        (COLOR GRAPHICS)"
1060 PRINT 3,"Y-Z PLANE        (COLOR GRAPHICS)"
1070 PRINT 4,"X-Y PLANE        (ASCII GRAPHICS)"
1080 PRINT 5,"X-Z PLANE        (ASCII GRAPHICS)"
1090 PRINT 6,"Y-Z PLANE        (ASCII GRAPHICS)"
1100 PRINT 7,"INPUT ANOTHER DATA SET OR QUIT"
1110 PRINT: INPUT "CHOICE";CHOICE
1120 CLS
1130 IF CHOICE <1 OR CHOICE >7 THEN GOTO 1020
1140 IF CHOICE =7 THEN GOTO 1170
1150 ON CHOICE GOSUB 1480,1730,1980,1480,1730,1980
1160 GOTO 1020
1170 PRINT "WOULD YOU LIKE TO INPUT ANOTHER DATA FILE?";"  TYPE Y/N"
1180 INPUT Q$
1190 IF Q$="Y" THEN GOTO 880
1200 IF Q$="N" THEN GOTO 1220
1210 GOTO 1170
1220 END
1230 REM*************************************************************************
1240 REM*                                SUB 1300                               *
1250 REM*                                                                       *
1260 REM*   This subroutine scales the dimensions of the simulator block to     *
1270 REM*      allow screen display.                                            *
1280 REM*                                                                       *
1290 REM*************************************************************************
1300 FOR IC=1 TO X
1310 XC(IC)=INT(XDIM(IC)*XSCALE)
1320 NEXT IC
1330 FOR JRC=1 TO Y
1340 YR(JRC)=INT(YDIM(JRC)*YRSCAL)
1350 YC(JRC)=INT(YDIM(JRC)*YCSCAL)
1360 NEXT JRC
1370 FOR KR=1 TO Z
1380 ZR(KR)=INT(ZDIM(KR)*ZSCALE)
1390 NEXT KR
1400 RETURN
```

```
1430 REM*                                                                      *
1440 REM*    This subroutine calls the subroutines needed to display the x-y   *
1450 REM*       slices.                                                        *
1460 REM*                                                                      *
1470 REM********************************************************************
1480 ROWS=Y
1490 COLS=X
1500 GOSUB 2230
1510 GOSUB 2340
1520 PRINT "YOU ARE IN THE X-Y PLANE MODE": PRINT
1530 PRINT "YOU HAVE A CHOICE OF ";Z,"  SLICES":PRINT
1540 PRINT "ENTER THE NUMBER OF THE DESIRED SLICE"
1550 PRINT "...OR ENTER 0 TO RETURN TO PLANE MENU": PRINT
1560 COLOR 7,0
1570 INPUT "SLICE";SLICE
1580 CLS
1590 IF SLICE>Z THEN GOTO 1570
1600 IF SLICE=0 THEN GOTO 1650
1610 K=SLICE
1620 GOSUB 2690
1630 GOSUB 3680
1640 GOTO 1560
1650 RETURN
1660 REM********************************************************************
1670 REM*                          SUB 1730                                  *
1680 REM*                                                                    *
1690 REM*    This subroutine calls the subroutines needed to display the x-z *
1700 REM*       slices.                                                      *
1710 REM*                                                                    *
1720 REM********************************************************************
1730 ROWS=Z
1740 COLS=X
1750 GOSUB 2230
1760 GOSUB 2560
1770 PRINT "YOU ARE IN THE X-Z PLANE MODE": PRINT
1780 PRINT "YOU HAVE A CHOICE OF ";Y,"  SLICES": PRINT
1790 PRINT "ENTER THE NUMBER OF THE DESIRED SLICE"
1800 PRINT "...OR ENTER 0 TO RETURN TO PLANE MENU": PRINT
1810 COLOR 7,0
1820 INPUT "SLICE";SLICE
1830 CLS
1840 IF SLICE>Y THEN GOTO 1820
1850 IF SLICE=0 THEN GOTO 1900
1860 J=SLICE
1870 GOSUB 2690
1880 GOSUB 3680
1890 GOTO 1810
1900 RETURN
1910 REM********************************************************************
1920 REM*                          SUB 1980                                  *
1930 REM*                                                                    *
1940 REM*    This subroutine calls the subroutines needed to display the y-z *
1950 REM*       slices.                                                      *
1960 REM*                                                                    *
1970 REM********************************************************************
1980 ROWS=Z
1990 COLS=Y
2000 GOSUB 2450
2010 GOSUB 2560
2020 PRINT "YOU ARE IN THE Y-Z PLANE MODE": PRINT
2030 PRINT "YOU HAVE A CHOICE OF ";X,"  SLICES": PRINT
2040 PRINT "ENTER THE NUMBER OF THE DESIRED SLICE"
```

```
2050 PRINT "...OR ENTER 0 TO RETURN TO PLANE MENU": PRINT
2060 COLOR 7,0
2070 INPUT "SLICE";SLICE
2080 CLS
2090 IF SLICE>X THEN GOTO 2070
2100 IF SLICE=0 THEN GOTO 2150
2110 I=SLICE
2120 GOSUB 2690
2130 GOSUB 3680
2140 GOTO 2060
2150 RETURN
2160 REM*************************************************************************
2170 REM*                              SUB 2230                                 *
2180 REM*                                                                       *
2190 REM*   This subroutine loads the display array when "x" represents the     *
2200 REM*      columns.                                                         *
2210 REM*                                                                       *
2220 REM*************************************************************************
2230 FOR XD=1 TO X
2240 WDTH(XD)=XC(XD)
2250 NEXT XD
2260 RETURN
2270 REM*************************************************************************
2280 REM*                              SUB 2340                                 *
2290 REM*                                                                       *
2300 REM*   This subroutine loads the display array when "y" represents the     *
2310 REM*      rows.                                                            *
2320 REM*                                                                       *
2330 REM*************************************************************************
2340 FOR YDR=1 TO Y
2350 LGTH(YDR)=YR(YDR)
2360 NEXT YDR
2370 RETURN
2380 REM*************************************************************************
2390 REM*                              SUB 2450                                 *
2400 REM*                                                                       *
2410 REM*   This subroutine loads the display array when "y" represents the     *
2420 REM*      columns.                                                         *
2430 REM*                                                                       *
2440 REM*************************************************************************
2450 FOR YDC=1 TO Y
2460 WDTH(YDC)=YC(YDC)
2470 NEXT YDC
2480 RETURN
2490 REM*************************************************************************
2500 REM*                              SUB 2560                                 *
2510 REM*                                                                       *
2520 REM*   This subroutine loads the display array when "z" represents the     *
2530 REM*      rows.                                                            *
2540 REM*                                                                       *
2550 REM*************************************************************************
2560 FOR ZD=1 TO Z
2570 LGTH(ZD)=ZR(ZD)
2580 NEXT ZD
2590 RETURN
2600 REM*************************************************************************
2610 REM*                              SUB 2690                                 *
2620 REM*                                                                       *
2630 REM*   This subroutine locates the appropriate areas on the screen to be  *
2640 REM*      filled.  It subsequently calls routines which assign color       *
2650 REM*      tags based on each saturation value, and locate each screen      *
2425 REM*      block to be colored.                                             *
2660 REM*                                                                       *
2670 REM*                                                                       *
```

```
2680 REM*************************************************************************
2690 NUMR=1
2700 NUMC=1
2710 RLMT=LGTH(1)
2720 CLMT=WDTH(1)
2730 FOR RR=1 TO ROWS
2740 FOR CC=1 TO COLS
2750 GOSUB 2950
2760 GOSUB 3340
2770 NUMC=CLMT+1
2780 CLMT=CLMT+WDTH(CC+1)
2790 NEXT CC
2800 NUMR=RLMT+1
2810 NUMC=1
2820 RLMT=RLMT+LGTH(RR+1)
2830 CLMT=WDTH(1)
2840 NEXT RR
2850 RETURN
2860 REM*************************************************************************
2870 REM*                              SUB 2950                                 *
2880 REM*                                                                       *
2890 REM*    This subroutine flags the saturation values in order to assign a   *
2900 REM*       value to a tag.  This value will determine what color or which  *
2910 REM*       ASCII character will be used to define that saturation on the   *
2920 REM*       screen or with hardcopy.                                        *
2930 REM*                                                                       *
2940 REM*************************************************************************
2950 IF CHOICE=1 OR CHOICE=4 THEN I=CC: J=RR
2960 IF CHOICE=2 OR CHOICE=5 THEN I=CC: K=RR
2970 IF CHOICE=3 OR CHOICE=6 THEN J=CC: K=RR
2980 IF SO(I,J,K)<=.45 THEN GOTO 3050
2990 IF SO(I,J,K)<=.5 AND SO(I,J,K)>.45 THEN GOTO 3080
3000 IF SO(I,J,K)<=.55 AND SO(I,J,K)>.5 THEN GOTO 3110
3010 IF SO(I,J,K)<=.6 AND SO(I,J,K)>.55 THEN GOTO 3140
3020 IF SO(I,J,K)<=.65 AND SO(I,J,K)>.6 THEN GOTO 3170
3030 IF SO(I,J,K)<=.7 AND SO(I,J,K)>.65 THEN GOTO 3200
3040 IF SO(I,J,K)<=1 AND SO(I,J,K)>.7 THEN GOTO 3230
3050 IF CHOICE<4 THEN COLR=COLRX(1): RETURN
3060 CHAR=CHARX(1)
3070 RETURN
3080 IF CHOICE<4 THEN COLR=COLRX(2): RETURN
3090 CHAR=CHARX(2)
3100 RETURN
3110 IF CHOICE<4 THEN COLR=COLRX(3): RETURN
3120 CHAR=CHARX(3)
3130 RETURN
3140 IF CHOICE<4 THEN COLR=COLRX(4): RETURN
3150 CHAR=CHARX(4)
3160 RETURN
3170 IF CHOICE<4 THEN COLR=COLRX(5): RETURN
3180 CHAR=CHARX(5)
3190 RETURN
3200 IF CHOICE<4 THEN COLR=COLRX(6): RETURN
3210 CHAR=CHARX(6)
3220 RETURN
3230 IF CHOICE<4 THEN COLR=COLRX(7): RETURN
3240 CHAR=CHARX(7)
3250 RETURN
```

```
3260 REM*************************************************************************
3270 REM*                              SUB 3340                                 *
3280 REM*                                                                       *
3290 REM*    This subroutine locates each character block on the screen to be   *
3300 REM*       filled.  It then will call one of two subroutines depending     *
3310 REM*       upon whether a color plot or character plot is desired.         *
3320 REM*                                                                       *
3330 REM*************************************************************************
3340 FOR RF=NUMR TO RLMT
3350 FOR CF=NUMC TO CLMT
3360 LOCATE RF,CF
3370 IF CHOICE<4 THEN GOSUB 3490: GOTO 3390
3380 GOSUB 3590
3390 NEXT CF
3400 NEXT RF
3410 RETURN
3420 REM*************************************************************************
3430 REM*                              SUB 3490                                 *
3440 REM*                                                                       *
3450 REM*    This subroutine colors each character block on the screen when a   *
3460 REM*       color plot is chosen.                                           *
3470 REM*                                                                       *
3480 REM*************************************************************************
3490 COLOR 15,COLR,7
3500 PRINT " "
3510 RETURN
3520 REM*************************************************************************
3530 REM*                              SUB 3590                                 *
3540 REM*                                                                       *
3550 REM*    This subroutine prints an ASCII character in each character block  *
3560 REM*       when a character plot is chosen.                                *
3570 REM*                                                                       *
3580 REM*************************************************************************
3590 PRINT CHR$(CHAR)
3600 RETURN
3610 REM*************************************************************************
3620 REM*                              SUB 3680                                 *
3630 REM*                                                                       *
3640 REM*    This subroutine generates a visual key.  Key generated will        *
3650 REM*       either be color key or character key depending on plot chosen.  *
3660 REM*                                                                       *
3670 REM*************************************************************************
3680 FORE=0
3690 KSTART=4
3700 KEND=10
3710 FOR KOUNT=1 TO 7
3720 FOR KKEY=KSTART TO KEND
3730 LOCATE 22,KKEY
3740 IF CHOICE>3 THEN PRINT CHR$(CHARX(KOUNT)): GOTO 3770
3750 IF KOUNT=7 THEN FORE=7
3760 COLOR FORE,COLRX(KOUNT)
3770 NEXT KKEY
3780 IF CHOICE>3 THEN LOCATE 23,KSTART: GOTO 3800
3790 LOCATE 22,KSTART
3800 ON KOUNT GOSUB 3910,3930,3950,3970,3990,4010,4030
3810 KSTART=KEND+1
3820 KEND=KSTART+10
3830 NEXT KOUNT
3840 RETURN
```

```
3850 REM*************************************************************************
3860 REM*                SUBS 3910,3930,3950,3970,3990,4010,4030                *
3870 REM*                                                                       *
3880 REM*   The remaining subroutines simply print a label key.                 *
3890 REM*                                                                       *
3900 REM*************************************************************************
3910 PRINT " <=.45 "
3920 RETURN
3930 PRINT " >.45&<=.5 "
3940 RETURN
3950 PRINT " >.5&<=.55 "
3960 RETURN
3970 PRINT " >.55&<=.6 "
3980 RETURN
3990 PRINT " >.6&<=.65 "
4000 RETURN
4010 PRINT " >.65&<=.7 "
4020 RETURN
4030 PRINT " >.7&<=1.0 "
4040 RETURN
Ok
```

★ U.S. GPO: 1988 561-025/80032